# UNIVERSITÄT BONN
# Physikalisches Institut


## First-order phase transitions and spinodal points in one-dimensional steady states


von

Peter Arndt



Phase transitions and spinodal points in steady states are investigated. A three-states (positive, negative particles and vacancies) one-dimensional reaction-diffusion model is studied by Monte-Carlo simulations and mean-field approximations. The model is $CP$ invariant, where $C$ denotes the interchange of positive and negative particles and $P$ the interchanges of left and right. A line of first-order phase transitions separates a phase where the symmetry is spontaneously broken and a $CP$-invariant phase. At the transition line the density profiles can be understood through an unexpected pattern of shocks. In the broken phase the free-energy functional is not convex, but behaves like a standard Ginzburg-Landau Potential under variations of the parameters of the model. Introducing a symmetry-breaking field one of the broken phases gets meta-stable or unstable. The time evolution is studied by diagonalization of the corresponding Hamilton operator associated with the master equation. There are massless excitations on the first-order transition line with a dynamical exponent $z = 2$. Two simplification of the model are defined and allow further analytical and numerical treatment. At the spinodal point the dynamical exponent $z = 1$ is found.



Post address:
Nussallee 12
53115 Bonn
Germany



BONN-IR-98-12
Bonn University
August 1998
ISSN-0172-8741

UNIVERSITÄT BONN
Physikalisches Institut

# First-order phase transitions and spinodal points in one-dimensional steady states

von
Peter Arndt

Dieser Forschungsbericht wurde als Dissertation von der Mathematisch - Naturwissenschaftlichen Fakultät der Universitiät Bonn angenommen.

Referent: Prof. Dr. V. Rittenberg
Korreferent: Prof. Dr. R. Flume
Tag der Promotion: 13. März 1998

Contents

## 1. Introduction

In the focus of this thesis are phenomena in non-equilibrium statistical mechanics. In contrast to equilibrium statistical mechanics, where the investigated system is in equilibrium with its environment (e.g. a heat bath), the non-equilibrium system may be driven by a "force" (e.g. a pump generating a constant flow). After a time such a system reaches its stationary state in which its properties show no time evolution any more. These states differ from equilibrium states in many ways and are able to show a much richer phenomenology. Typical questions concern the identification of appropriate variables as well as the study of their stationary and time-dependent properties, such as means, fluctuations, correlations and response to external fields.

For systems in thermal equilibrium, this approach is well established by virtue of the framework provided by Gibbs [1]. Once a microscopic Hamiltonian $H$ of the system is specified, the equilibrium distribution over the configuration space is known in terms of the familiar Boltzmann factor, $\exp(-H/k_{\mathrm{B}}T)$, where $T$ is the temperature and $k_{\mathrm{B}}$ the Boltzmann constant. Thus, averages of time-independent observables can be computed, at least in principle.

It is well known that systems may abruptly change their macroscopic behaviour as some parameters are smoothly varied. The points at which this happens are called critical points, and they usually mark a phase transition. There are basicly two possible ways, in which such a transition may occur. In the first scenario, two phases coexist at the critical point. Slightly away from the critical point, however, there is generally a unique phase whose properties are continuously connected to one of the coexistent phases at the critical point. In that case, we expect discontinuous behaviour in various quantities as we pass through the critical point and therefore from one stable phase to another. Such a transition is termed *first-order*. Melting of a solid is a well-known example for such a transition.

The other type of transition is the continuous or *second-order* phase transition. For these transitions the two phases, above and below the critical point, become identical as the transition point is approached. This behaviour is accompanied by the divergence of the correlation length. This is the length scale of correlations in the system (e.g. a few interatomic spacings in a solid away from criticality). Due to the divergence of this scale, fluctuations are correlated over the whole system.

A simple example for such a transition is a ferromagnet at the Curie temperature $T_{\mathrm{C}}$. The two interesting parameters in this system which may be varied are the temperature $T$ and the external magnetic field $H$. There is a line of first-order phase transitions ($H = 0, T < T_{\mathrm{C}}$), which gets second order at $T = T_{\mathrm{C}}$. When $T < T_{\mathrm{C}}$, the magnetization is discontinuous, the two limits $H \to 0+$ and $H \to 0-$ give two different non-zero values of magnetizations $\pm M_0$. At the line of first-order phase transitions *spontaneous symmetry breaking* occurs: Although the system is symmetric under reversal of all local magnetic degrees of freedom, this symmetry is not respected by the equilibrium state. A mixture of the two phases, spatially separated by Bloch walls, is observed. At the Curie point, the magnetization vanishes, it serves as an order parameter for this transition.

The situation is quite different for systems not in equilibrium. These systems are often defined through their dynamics. They show a wide range and enormous complexity of behaviour. Therefore, a reasonable classification scheme has not been found yet.

In contrast to equilibrium, the distribution function is time-dependent, obeying say a master equation. One way of investigation is to study a system which settled down into its non-equilibrium stationary state, such that the distribution $P(\sigma)$ has become time-independent while non-Hamiltonian, i.e. it cannot be written as $\exp(H(\sigma))$ with a given Hamiltonian $H$. This distribution does not have to fulfil a detailed balance condition. It shows amongst other new also known behaviour from equilibrium states, like the occurrence of critical points, phase transitions and spontaneous symmetry breaking. But these states are much more difficult to analyse. Many powerful concepts as the free energy or entropy description of a system are not at ones hand and equally powerful concepts appropriate for non-equilibrium behaviour have not been found yet. But, carefully defined, the free energy can be of much help even in non-equilibrium systems. There is poor knowledge about alternative methods which can be applied.

To consider a natural non-equilibrium system like a chemical reaction in an open vessel in all its details is a hopeless task. But due to the phenomenon of *universality* in critical behaviour, i.e. that critical behaviour depends only on a very few fundamental parameters, like the symmetries and the dimensionality of the problem, one may study a simple model while still capturing the essential physics of the system. In the field of non-equilibrium systems, reaction-diffusion models play a paradigmatic role [2, 3]. One assumes that the particles are located on a lattice, on which they can move and interact with each other. The model may be found in a configuration $\sigma$, which is defined by the position of all particles on the lattice. The stochastic dynamic of the model can be defined by means of transition rates $\Gamma_{\sigma\to\tau}$ from a configuration $\sigma$ to a configuration $\tau$. The probability $P(\sigma,t)$ to find the model in a configuration $\sigma$ at time $t$ then fulfils the *master equation*

$$\frac{\mathrm{d}}{\mathrm{d}t}P(\sigma,t)=\sum_{\gamma}\Gamma_{\gamma\to\sigma}\,P(\gamma,t)-\sum_{\delta}\Gamma_{\sigma\to\delta}\,P(\sigma,t)\,.$$

This is first-order differential equation for $P(\sigma,t)$, which have to be solved for a given initial condition $P(\sigma,t=0)$. The first term on the rhs. describes a flow of probability into the configuration $\sigma$ while the second describes the flow out of this configuration into other configurations $\delta$.

A vast of reaction-diffusion models have been studied already. They can be grouped together either by their dimensionality, their number of types of particles, their symmetries, their conservation laws (e.g. particle conservation) or by the method of investigation (e.g. analytical, by a coarse grained Langevin approach, mean-field approximations or Monte Carlo simulations). Analytical results are known for some one-dimensional two-state models, as the totally [4, 5, 6, 7, 8] or partially [9] asymmetric exclusion process. These results were obtained by a matrix product ansatz for the stationary probability distribution, which can be extended to three and more states [10, 11]. At this point interesting mathematics occur, namely the existence and representation of quadratic algebras. Further aspects of such models or variations of this ansatz are studied in [12, 13, 14, 15]. A particular interesting result is that of [16], where it is shown that any stationary probability distribution of an open system can be expressed through an appropriate product of matrices fulfilling quadratic relation given through the dynamics of the model.

More complicated models, especially in two or more dimensions, can only be studied by approximative methods [17, 18, 19].

Here, we want to investigate an one-dimensional non-equilibrium model which shows a first-order phase transition and spontaneous symmetry breaking. It is well known that systems in thermal equilibrium do not exhibit spontaneous symmetry breaking in one dimension at finite temperature, provided that the interactions are short range and that the local variable which describes the microscopic state of the system takes only a finite number of possible values [20, 21]. Establishing spontaneous symmetry breaking in a non-equilibrium model is more difficult than in an equilibrium one, since, due to the ergodicity of finite systems, the former one will flip between the two spontaneously broken phases. This is a remarkable phenomena of non-equilibrium systems only, since those have the possibility of temporal phase separation, in contrast to equilibrium systems, where the phases have to separate in space. In non-equilibrium one has to study the decay times of such phases, which for a model with spontaneous symmetry breaking should increase at least with the dimension of the space of configurations. The introduction of an external field which breaks the symmetry of the model enables us to consider spinodal points and the stability or meta-stability of a state, which is not possible for equilibrium systems, which are time-independent. Thus, the simple model studied here demonstrates already a richer physics as an equilibrium model. Besides the investigation of stationary properties it is even possible to study the time evolution of the model.

It will be shown that a free energy functional can be defined, which helps us to establish the first-order phase transition in this model. This phase transition is studied in more detail and shock configurations are found.

The presentation of results [22, 23] is organized in three chapters, which are followed by a conclusion. In the next chapter the above mentioned model is defined. It is a three-state diffusion model, which only in a special case can be treated analytically [10, 24]. Therefore it will be studied by a mean-field approximation first (section 2.1). It will turn out that the phase diagram given through the mean-field results is partially wrong. This is quite surprising, since in other models, the mean-field approximation gives the right phase diagram [25]. We will then rely on Monte Carlo simulations and establish the first-order phase transition and spinodal points.

To study the model in the broken phases in more detail, the model is simplified to a random walker on a triangle (RWT model) in chapter 3. The spectrum of the time evolution and the movement of the random walker can be investigated and universal behaviour is found at the spinodal point.

In chapter 4 the RWT model is simplified further to a random walker on a right angle (RWRA model). This model can be analysed analytically, and still captures the essential physics of the three-state diffusion model in the broken domain.

## 2. The three-state diffusion model

Several years ago Krug [26] suggested the existence of boundary induced phase transitions in one-dimensional steady states. A line of first-order phase transitions (the so-called coexistence line) was found in the two-state asymmetric exclusion model [5, 6, 27] in which particles (call them positive) hop among vacancies (call them negative particles). On the coexistence line, the system is $CP$-symmetric ($C$ corresponds to changing the sign of the particles, $P$ is the parity operation) and the symmetry is spontaneously broken. Since we want to compare the nature of the phase transitions in equilibrium and non-equilibrium phenomena, the phase transition just described would correspond to the two-dimensional $n$-state Potts model [28] with $n > 4$ at the critical temperature. The exclusion model does not have the equivalent of the low temperature domain which corresponds to the broken phase.

The three-state diffusion model of Evans, Foster, Godrèche and Mukamel [24, 29] presents a broken phase (the equivalent of the low temperature domain of the $n$-states Potts models) and this motivated us to study this model in detail. Through our investigation several new and previously unknown effects were observed.

The model is defined through its stochastic dynamics. Each site of an one-dimensional lattice with $L$ sites may be occupied by a positive particle or a negative particle or be empty. In each infinitesimal time step $\mathrm{d}t$ the following events may occur at each pair of nearest-neighbour sites $k$, $k+1$:

$$\begin{aligned}
&(+)_k\,(\,0\,)_{k+1} \to (\,0\,)_k\,(+)_{k+1}\\
&(+)_k\,(-)_{k+1} \to (-)_k\,(+)_{k+1}\\
&(\,0\,)_k\,(-)_{k+1} \to (-)_k\,(\,0\,)_{k+1}
\end{aligned} \tag{2.1}$$

all with probability $\mathrm{d}t$. Where $(+)_k$, $(-)_k$ and $(\,0\,)_k$ denote a positive particle, a negative particle or a vacancy at the site $k$. In the same time step $\mathrm{d}t$ the following events may occur at the left boundary ($k = 1$)

$$\begin{aligned}
&(\,0\,)_1 \to (+)_1 \quad \text{with probability } \alpha\ \mathrm{d}t\\
&(-)_1 \to (\,0\,)_1 \quad \text{with probability } \beta(1-h)\ \mathrm{d}t
\end{aligned} \tag{2.2}$$

and at the right boundary ($k = L$)

$$\begin{aligned}
&(\,0\,)_L \to (-)_L \quad \text{with probability } \alpha\ \mathrm{d}t\\
&(+)_L \to (\,0\,)_L \quad \text{with probability } \beta(1+h)\ \mathrm{d}t\ .
\end{aligned} \tag{2.3}$$

One notices that for $h = 0$ the probabilities are $CP$-invariant.

The time evolution of the system is given by a master equation or its equivalent imaginary time Schrödinger equation [2, 9]

$$\frac{\mathrm{d}}{\mathrm{d}t}|P> = -H\,|P> \tag{2.4}$$

where $|P>$ is the probability vector and $H$ is the Hamiltonian of an one-dimensional quantum chain, which should not be mistaken as a Hamiltonian of a Gibbs ensemble in equilibrium statistical mechanics.

The time evolution operator $H$ of the master equation (2.4) for the processes (2.1)–(2.3) can be written as a sum of operators acting non-trivially on adjacent sites (hopping) and of two operators acting on the first and last site (input and output):

$$H = H_1 + \sum_{k=1}^{L-1} H_{k,k+1} + H_L \, . \tag{2.5}$$

The matrices are

$$H_{k,k+1} = I_1 \otimes \cdots \otimes I_{k-1} \otimes \begin{pmatrix} 0 & 0 & 0 & 0 & 0 & 0 & 0 & 0 & 0 \\ 0 & 0 & 0 & -1 & 0 & 0 & 0 & 0 & 0 \\ 0 & 0 & 1 & 0 & 0 & 0 & 0 & 0 & 0 \\ 0 & 0 & 0 & 1 & 0 & 0 & 0 & 0 & 0 \\ 0 & 0 & 0 & 0 & 0 & 0 & 0 & 0 & 0 \\ 0 & 0 & 0 & 0 & 0 & 1 & 0 & 0 & 0 \\ 0 & 0 & -1 & 0 & 0 & 0 & 0 & 0 & 0 \\ 0 & 0 & 0 & 0 & 0 & -1 & 0 & 0 & 0 \\ 0 & 0 & 0 & 0 & 0 & 0 & 0 & 0 & 0 \end{pmatrix}_{k,k+1} \otimes I_{k+2} \otimes \cdots \otimes I_L$$

$$H_1 = \begin{pmatrix} \alpha & 0 & -\beta(1-h) \\ -\alpha & 0 & 0 \\ 0 & 0 & \beta(1-h) \end{pmatrix}_1 \otimes I_2 \otimes \cdots \otimes I_L$$

$$H_L = I_1 \otimes \cdots \otimes I_{L-1} \otimes \begin{pmatrix} \alpha & -\beta(1+h) & 0 \\ 0 & \beta(1+h) & 0 \\ -\alpha & 0 & 0 \end{pmatrix}_L \tag{2.6}$$

where the subscripts denotes the sites the matrices act on, and $I$ is the $3 \times 3$ unit matrix. The order of the basis at each site is chosen as $|\,0\!>$, $|\!+\!>$, $|\!-\!>$. Note that $H$ is not hermitian.

In the next four sections, we are interested in stationary state properties only. We define $p(k)$, $m(k)$ and $v(k)$ as the steady state density of positive, negative particles and vacancies at the site $k$, respectively. Their average values being $p$, $m$ and $v$. It is also useful to define the quantities

$$\begin{aligned} d(k) &= p(k) - m(k) \\ s(k) &= (p(k) + m(k))/2 \, , \end{aligned} \tag{2.7}$$

their average values being $d$ and $s$. The latter five averaged quantities can serve as order parameters. Especially, $d$ is connected to the *CP* symmetry since it changes sign under its action. In the following, we will also see that the average densities $p$ and $m$ are also realized in a macroscopic region of lattice and therefore are measurable.

An useful tool in the later analysis is the free energy functional which is defined as follows [30]: Take an order parameter $w$ and let $P(L, w)$ be the probability to have $w$ for a lattice with $L$ sites. Defining

$$f_L(w) = -\frac{1}{L} \log P(L, w) \tag{2.8}$$

the free energy functional (FEF) is

$$f(w) = \lim_{L \to \infty} f_L(w) \, . \tag{2.9}$$

For equilibrium systems this is a convex function. As we are going to see in section 2.2, this is not true for stationary states which do not describe Gibbs ensembles. In the region of the broken phases, if we take $d$ as order parameter the FEF looks like a Ginzburg-Landau picture in the case of spontaneous breaking of a symmetry [31].

We have also looked at the spectrum of the Hamiltonian (2.5) on the separation line. It is gapless with a critical dynamical exponent [32] $z = 2$. This suggests, from the experience with the one-species model, the existence of shocks [33, 34]. Some of the ideas developed here are already in the paper of Bennett and Grinstein [35].

In section 2.3 we study in detail (for $\alpha = 1$) the nature of the first-order phase transition. A novel feature comes from the fact that we have not one but two order parameters ($p$ and $m$ or $s$ and $d$). In the $p$-$m$ plane the minima of the FEF lie on a boomerang like figure. We show how this figure can be obtained by an interesting combination of shocks. The existence of shocks allows the prediction of linear density profiles which are indeed observed in several Monte Carlo simulations.

In section 2.4 we consider the effect of a symmetry breaking term on the process (we take $h$ greater than zero for the processes (2.2)–(2.3)). We show that the FEFs look like text book Ginzburg-Landau pictures including the existence of spinodal points in the broken phases. As it is well known [36], such points do not exist in equilibrium phenomena. The mean-field approximation are compared here with the Monte Carlo simulations. Apparently, mean-field theory gives a good approximation to the data only for small values of $\beta$ and large values of $h$.

Moreover, we show that the spectrum of the Hamiltonian shows massless excitations at the spinodal point with a dynamical critical exponent $z = 1$. This is a very surprising result for stochastic processes. This exponent is typical for continuous equilibrium phase transitions.

### 2.1. *Mean-field theory*

First we present the mean-field theory of the model. We will see that depending on the parameters $\alpha$, $\beta$ and $h$ the system of mean-field equations admits one or several solutions with different physical properties.

Let us define the number operators $\pi_k$ and $\mu_k$ which count the number of positive and negative particles at site $k$, respectively ($\pi_k, \mu_k \in \{0, 1\}$). In the mean-field approximation any correlations are ignored, and we write any two-point correlation function as the product of the corresponding one-point functions, e.g.

$$<\pi_k \pi_j> = <\pi_k><\pi_j> \tag{2.10}$$

$$<\pi_k \mu_j> = <\pi_k><\mu_j> . \tag{2.11}$$

For notational simplicity we introduce the mean-field densities for the positive and negative particles as

$$p(k) = <\pi_k> \tag{2.12}$$

$$m(k) = <\mu_k> . \tag{2.13}$$

In the stationary state the local currents between sites $k$ and $k+1$ of positive or negative particles are the same for each $k$ and we find

$$j^+ = \alpha(1 - p(1) - m(1)) = p(k)(1 - p(k+1)) = \beta(1 + h)p(L) \tag{2.14}$$

$$j^- = \beta(1 - h)m(1) = m(k+1)(1 - m(k)) = \alpha(1 - p(L) - m(L)). \tag{2.15}$$

For the bulk ($1 \leq k < L$), these equations decouple and introducing

$$\beta^{\pm} = \beta(1 \pm h) \tag{2.16}$$
$$\alpha^{+} = \frac{\alpha(1 - p(1) - m(1))}{1 - p(1)} = \frac{j^{+}}{j^{+}/\alpha + j^{-}/\beta^{-}} \tag{2.17}$$
$$\alpha^{-} = \frac{\alpha(1 - p(L) - m(L))}{1 - m(L)} = \frac{j^{-}}{j^{-}/\alpha + j^{+}/\beta^{+}} \tag{2.18}$$

the problem of solving equations (2.14) and (2.15) is reduced to solving two models each with one type of totally asymmetric diffusing particles and with input and output rates $\alpha^{+}, \beta^{+}$ and $\alpha^{-}, \beta^{-}$, respectively.

The latter process is called the totally asymmetric exclusion process (TAEP) and mean-field and exact solutions are known [5, 25]. Depending on $\alpha^s$ and $\beta^s$ ($s = \pm$) the model is in one of four phases. These phases are

- *the power-law phase* for $\alpha^s > 1/2$ and $\beta^s > 1/2$. The current in this phase is $j^s = 1/4$ and the bulk density is $\rho^s = 1/2$.
- *the low-density phase* for $\alpha^s < 1/2$ and $\beta^s > \alpha^s$. The current is $j^s = \alpha^s(1 - \alpha^s)$ and $\rho^s = \alpha^s$ in the bulk.
- *the high-density phase* for $\beta^s < 1/2$ and $\alpha^s > \beta^s$. Here one has $j^s = \beta^s(1 - \beta^s)$ and $\rho^s = 1 - \beta^s$.
- *the coexistence line* for $\alpha^s = \beta^s < 1/2$. The current is $j^s = \alpha^s(1 - \alpha^s)$.

Each of the decoupled chains is in one of these phases. Depending on $\alpha$, $\beta$ and $h$, only certain combinations of phases can occur, since the two chains are still coupled through the boundaries (2.17) and (2.18).

Let us first consider the *CP*-symmetric phases of the three-state model. The current of positive particles have to be equal to the current of negative particles, $j^{+} = j^{-}$. In this case, equations (2.17) and (2.18) simplify to

$$\alpha^{+} = \frac{\alpha\beta^{-}}{\alpha + \beta^{-}} \tag{2.19}$$
$$\alpha^{-} = \frac{\alpha\beta^{+}}{\alpha + \beta^{+}}. \tag{2.20}$$

One finds

∘ *the power-law symmetric phase.*
In this phase both currents are $j^{+} = j^{-} = 1/4$ and the densities of the particles is $p = m = 1/2$. We find this phase for

$$\alpha^s > 1/2, \qquad \beta^s > 1/2. \tag{2.21}$$

These conditions reduce to

$$\beta > \frac{1}{1-h}\,\frac{\alpha}{2\alpha - 1}, \qquad \alpha > 1/2. \tag{2.22}$$

∘ *the low-density symmetric phase.*
For $h = 0$ there exists a symmetric low-density phase with $\alpha^{+} = \alpha^{-}$ and hence $j^{+} = j^{-} = \alpha^{+}(1 - \alpha^{+})$. The conditions for this phase are

$$\alpha^s < 1/2, \qquad \alpha^s < \beta^s. \tag{2.23}$$

For the densities of positive and negative particles we find

$$p = m = \frac{\alpha\beta}{\alpha+\beta} < \frac{1}{2} \tag{2.24}$$

If we turn on the asymmetry $h$, this phase does not exist anymore. Instead, one finds a phase with the two types of particles in the low-density phase of the two-state TAEP chain but with different currents. One has to distinguish between the favoured and unfavoured low-density/low-density phase.

∘ *the favoured low-density/low-density phase.*
A positive $h$ favours the output of positive particles, such that more negative particles can be injected. Therefore the current of negative particles is likely to be greater than the current of positive particles. For the existence of the favoured low-density/low-density phase we require

$$j^+ = \alpha^+(1-\alpha^+) < j^- = \alpha^-(1-\alpha^-) \tag{2.25}$$

and need a solution of (2.17) and (2.18), which can be rewritten as

$$\alpha^+ = 1 - \frac{1}{\alpha}\alpha^+(1-\alpha^+) - \frac{1}{\beta^-}\alpha^-(1-\alpha^-) \tag{2.26}$$

$$\alpha^- = 1 - \frac{1}{\alpha}\alpha^-(1-\alpha^-) - \frac{1}{\beta^+}\alpha^+(1-\alpha^+), \tag{2.27}$$

with

$$\begin{aligned} &\alpha^+ < 1/2, && \alpha^- < 1/2 \\ &\beta^+ > \alpha^+, && \beta^- > \alpha^- \\ &\alpha^- > \alpha^+. && \end{aligned} \tag{2.28}$$

The set of quadratic equations (2.26) and (2.27) can be solved numerically only.

∘ *The unfavoured low-density/low-density phase*
occupies a smaller region in the phase diagram and can be found where a solution of (2.26) and (2.27) under the conditions (2.28) with $\alpha^+ > \alpha^-$ instead of $\alpha^- > \alpha^+$ exists. The respective region in the phase diagram shrinks with increasing $h$, since the asymmetry favours the other low-density/low-density phase.

∘ *The broken low-density/low-density phases for $h = 0$*
For $h = 0$, one finds two *CP*-broken phases i.e. there are two solutions to the mean-field equations (2.17) and (2.18) with $\alpha^\pm < 1/2$, $\alpha^\pm < \beta^\pm$ and $j^+ \neq j^-$ . The respective densities of particles is given through

$$\begin{aligned} s &= 2\left(1 - \frac{\alpha\beta}{\alpha-\beta}\right) \\ d &= \pm 2\left[(s-1)(\frac{\alpha\beta}{\alpha-\beta} - s)\right]^{\frac{1}{2}}, \end{aligned} \tag{2.29}$$

where $s$ and $d$ are defined above (2.7).

∘ *The broken high-density/low-density phases for $h = 0$*
For $h = 0$ one finds more *CP*-broken phases. In these phases one type of particles is in the

low-density phase of the TAEP the other in the high-density phase. The conditions upon $\alpha^\pm$ and $\beta^\pm$ are

$$
\begin{array}{ll}
\alpha^+ > 1/2, & \alpha^- < 1/2 \\
\beta^+ < \alpha^+, & \beta^- > \alpha^-.
\end{array}
$$

or

$$
\begin{array}{ll}
\alpha^+ < 1/2, & \alpha^- > 1/2 \\
\beta^+ > \alpha^+, & \beta^- < \alpha^-
\end{array}
$$

In the first case (the positive particles are in the high-density phase, the negative in the low-density phase) the densities are given by

$$
\begin{aligned}
p &= 1-\beta \\
m &= \frac{1+\alpha}{2} - \frac{1}{2}\left[(1+\alpha)^2 - 4\alpha\beta\right]^{\frac{1}{2}}
\end{aligned}
\tag{2.30}
$$

∘ *The favoured high-density/low-density phase*

For $h \neq 0$ one has again to distinguish between the favoured and unfavoured high-density/low-density phases. The phase where the negative particle is in the high-density phase is favoured, since the input of negative particles is enhanced and it is more probable to find a high density of negative particles. The positive particles are in the low-density phase and we have

$$
j^+ = \alpha^+(1-\alpha^+), \quad j^- = \beta^-(1-\beta^-). \tag{2.31}
$$

The solutions of (2.17) and (2.18) have to fulfil

$$
\begin{array}{ll}
\alpha^+ < 1/2, & \beta^- < 1/2 \\
\beta^+ > \alpha^+, & \beta^- < \alpha^-.
\end{array}
\tag{2.32}
$$

∘ *The unfavoured high-density/low-density phase*

For small $\beta$ and $h > 0$ it is possible, though not likely, to find the positive particles in the high-density phase and the negative in the low-density phase. In this case one has

$$
j^+ = \beta^+(1-\beta^+), \quad j^- = \alpha^-(1-\alpha^-). \tag{2.33}
$$

Such states are possible in a region of the phase diagram where the solutions of (2.17) and (2.18) fulfil

$$
\begin{array}{ll}
\beta^+ < 1/2, & \alpha^- < 1/2 \\
\alpha^+ > \beta^+, & \alpha^- < \beta^-.
\end{array}
\tag{2.34}
$$

Since it is not favoured by the asymmetry $h$ to find the system in this phase the respective region is smaller than for the favoured high-density/low-density phase and shrinks with increasing $h$. In the limit $\beta \to 0$ equations (2.34) and (2.34) can be replaced by

$$
h < \frac{1}{1+2\alpha}. \tag{2.35}
$$

This reveals the proposition in [37] for the critical point in the simplified RWT model.

◦ *The low-density/power-law phase*
This phase does not occur in the original model with $h = 0$. But for $h > 0$ one finds a phase where the negative particle is in the power-law phase and the positive is in the low-density phase. The conditions for this are

$$\begin{aligned} &\alpha^+ < 1/2, &&\alpha^- > 1/2 \\ &\beta^+ > \alpha^+, &&\beta^- > 1/2. \end{aligned} \tag{2.36}$$

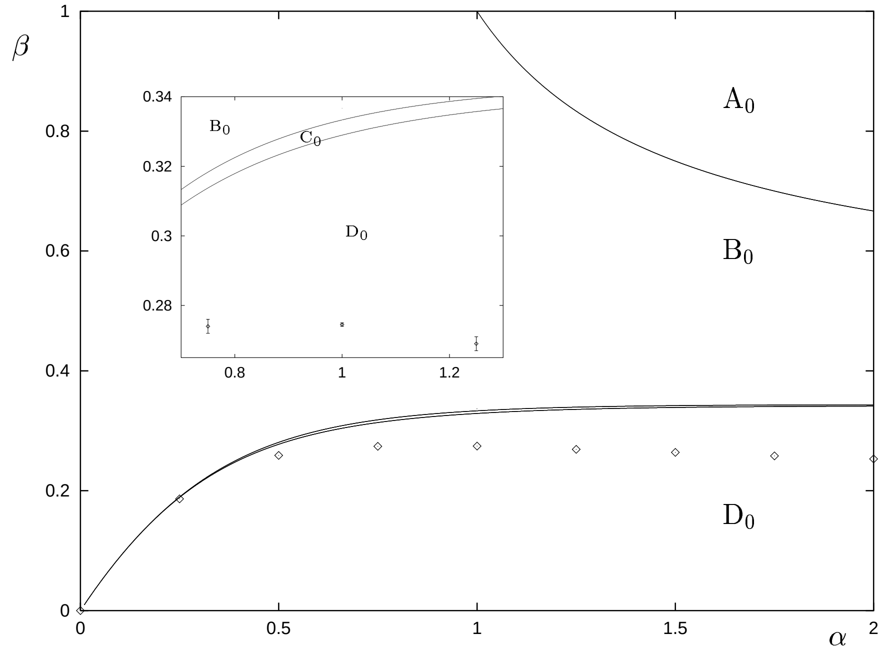


**Figure 1.** Phase diagram for $h = 0$. The region $A_0$, $B_0$, $C_0$ and $D_0$ are obtained in mean-field and defined in the text. Since the C phase is very narrow it is shown in an insert. The diamonds describe the boundary between the phase $\tilde{B}$ and the phase $\tilde{D}$ as obtained in Monte Carlo simulations. (No phase $C_0$ is observed.)

All phases mentioned fill the whole $\alpha$-$\beta$ plane. For the *CP*-symmetric case the mean-field phase diagram is shown in figure 1. In region $A_0$ one finds the power-law phase, in region $B_0$ the symmetric low-density phase, in region $C_0$ the broken low-density/low-density phases and in region $D_0$ the broken high-density/low-density phases. Note that the symmetric low-density phase is also found in regions $C_0$ and $D_0$. An exact calculation [24] using the matrix product ansatz for the wave function on the line $\beta = 1$ has confirmed the existence of phases $A_0$ and $B_0$. Limited Monte Carlo simulations [24] showed a strong similarity between the true and mean-field phase diagrams for $\alpha = 1$. Since for the two-species model [5, 6, 9, 27, 38] the phase diagram obtained by mean-field is exact, it might be tempting to conclude that in the present case the mean-field phase diagram is exact.

For $h > 0$ most of the above conditions lead to coupled quadratic equations like (2.26) and (2.27), which in general cannot be solved exactly. For $h = 0.1$ they were solved numerically

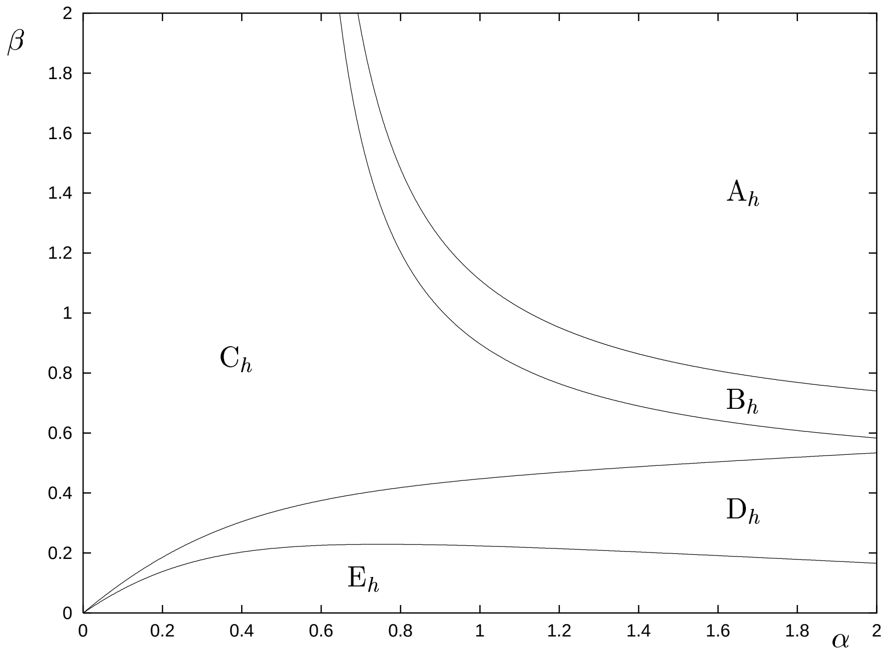


**Figure 2.** Phase diagram of the original model with asymmetry $h = 0.1$. The regions are obtained by mean-field and defined in the text.

and the obtained diagram is shown in figure 2. In the upper right corner the system is in the power-law phase ($\mathrm{A}_h$). Varying the parameters from there first the positive particles ($\mathrm{B}_h$) and then both type of particles ($\mathrm{C}_h$) change to the low-density phase. For small $\beta$ one finds the favoured high-density/low-density phase ($\mathrm{D}_h$,$\mathrm{E}_h$). The conditions for the unfavoured low-density/low-density and high-density/low-density are simultaneously fulfilled in the region ($\mathrm{E}_h$). Increasing the asymmetry this region shrinks, whereas the regime $\mathrm{D}_h$ grows. Note, that in E three different phases are allowed.

For $h \to 0$ the regimes $\mathrm{D}_h$ and $\mathrm{E}_h$ coincide and $\mathrm{B}_h$ vanishes. The low-density/low-density phases in $\mathrm{C}_h$ and $\mathrm{E}_h$ get symmetric ($j^+ = j^-$) for $h = 0$, and only a small strip of a *CP*-broken low-density/low-density phase remains between $\mathrm{C}_h$ and $\mathrm{D}_h$ giving the region $\mathrm{C}_0$ for $h = 0$.

To check the mean-field phase diagram we simulated the model. The results are presented in the next section.

### *2.2. The phase transition between the broken and unbroken phases*

In order to clarify the phase structure of the model, let us take $\alpha = 1$. (This is a vertical line in figure 1). If one wants to compare equilibrium with non-equilibrium phenomena, it is useful to have in mind the two-dimensional $n$-state Potts model with $n > 4$ and interpret the parameter $\beta$ as a temperature. Mean-field gives the following values of $\beta$ for the separations among the various phases:

- $\beta = 0.3289$ (between the high-density/low-density phases ($\mathrm{D}_0$) and the low-density/low-density phases ($\mathrm{C}_0$))

- $\beta = 0.3333 = 1/3$ (between the low-density/low-density phases ($C_0$) and the symmetric low-density phase ($B_0$))
- $\beta = 1$ (between the symmetric low-density phase ($B_0$) and the power-law phase ($A_0$))

In order to check the mean-field predictions we have done Monte Carlo simulations to get $f_L(d)$ taking $d$ (the difference between the averages of positive and negative particles) as order parameter.

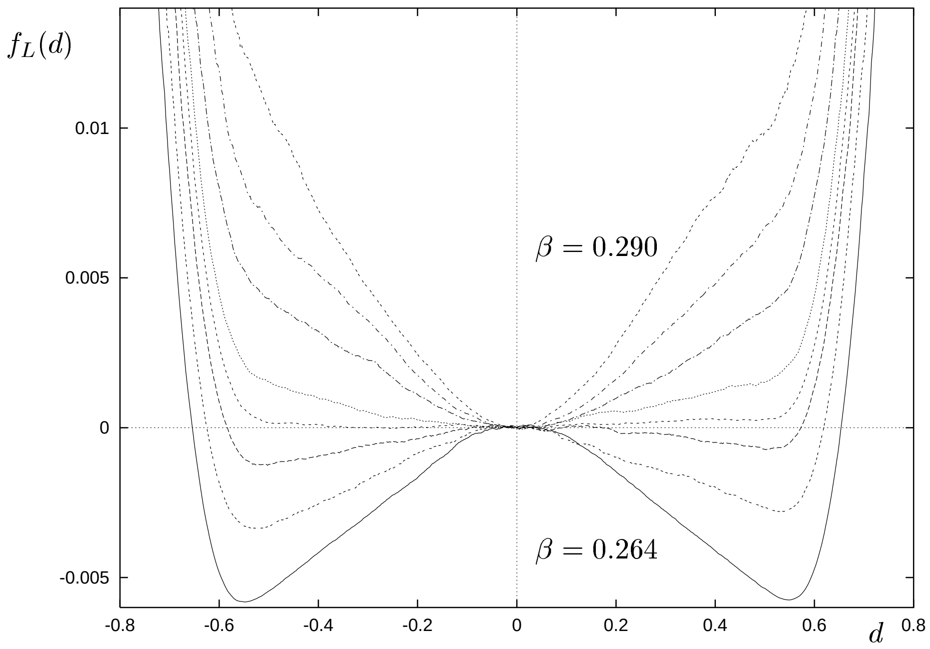


**Figure 3.** $f_L(d)$ for $\beta$ =0.264, 0.270, 0.274, 0.276, 0.280, 0.285, 0.290 and $L = 400$ sites. The values of $f_L(d)$ are shifted by their value $f_L(0)$.

In figure 3 we show our results for $L = 400$ and different values of $\beta$ (all belonging to the region $D_0$ in figure 1). In order to present the data in a clearer way, we have subtracted the values of $f_L(0)$ from $f_L(d)$. The data shown in figure 3 are interesting for two reasons: the shape of the FEF and the failure of mean-field predictions. First we notice that a dramatic change occurs around $\beta = 0.274$. As will be shown below the precise value is $\beta_{\mathrm{crit}} = 0.275$. Below $\beta_{\mathrm{crit}}$ the FEF is not a convex function, it has the behaviour of a text-book Ginzburg-Landau picture, and shows two minima at the values given by mean-field, see equation (2.30).

At $\beta_{\mathrm{crit}}$ the FEF behaves like the FEF of an equilibrium first-order phase transition. For $\beta > \beta_{\mathrm{crit}}$ the FEF is strictly convex and has the expected behaviour for a disordered phase. Notice that all the changes in the behaviour of $f_L(d)$ occur at values of $\beta$ below the value 0.3289 where, according to mean-field, the transition between the low-density/low-density and high-density/low-density phases is supposed to take place.

In order to make sure that we are not dealing with finite-size effects we have computed $f_L(d)$ for $\beta = 0.3$ (still below 0.3289) for various number of sites up to $L = 1000$. The data are shown in figure 4 (we have subtracted the value $f_L(0)$). One can see that $f_L(d)$ is practically independent of $L$. The value $f_L(0)$ is of order $1/L$ due to surface effects. This implies that

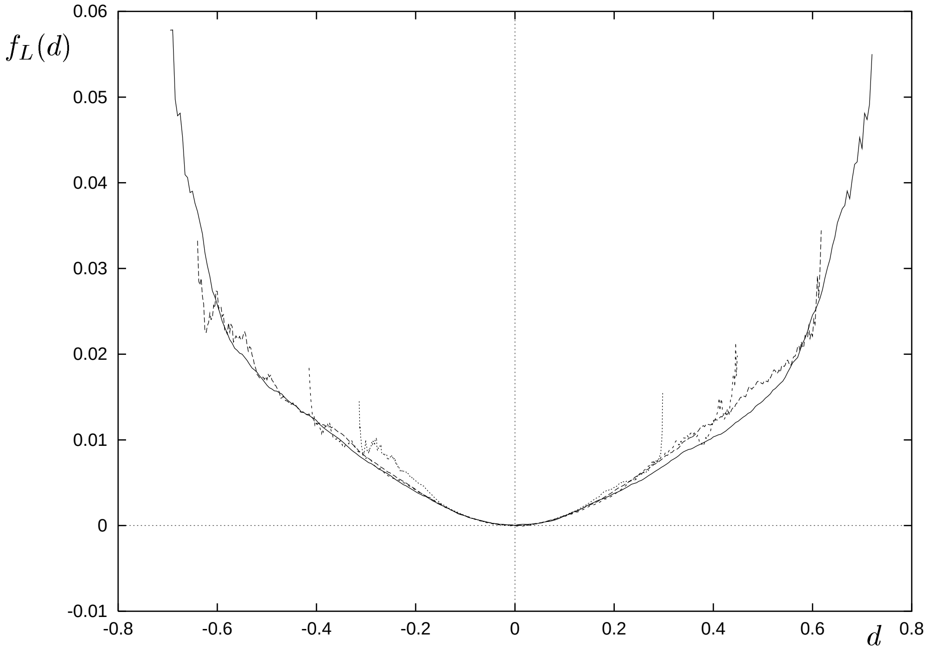


**Figure 4.** Free energy functional for $\beta = 0.3$: $f_L(d)$ for $L$ =200, 400, 600 and 1000 sites. The values of $f_L(d)$ for different $L$ are shifted by $f_L(0)$. The little vertical stretches of the curves are due to the limited CPU time of the Monte Carlo runs.

one does not have finite-size effects, and that $f_L(d) - f_L(0)$ is a strictly convex function with one minimum as one expects to have if one is in the "disordered" phase.

We now present more data which show what goes wrong with the mean-field prediction. In figure 5 we show the positions of the minima of $f_L(d)$ for various numbers of sites and various values of $\beta$. One can observe that below $\beta_{\rm crit}$ the minima converge to their mean-field values obtained from equation (2.30) and that a dramatic change takes place at $\beta_{\rm crit}$. Above $\beta_{\rm crit}$ the $CP$ symmetry is not broken anymore ($d = 0$).

In figure 6 we show the minima of $f_L(s)$ ($s = (p+m)/2$) as a function of $\beta$ for various $L$. The upper curve is given by the average value of $s$ for the broken high-density/low-density phases. This value is obtained from equation (2.30):

$$s = \frac{1-\beta}{2} + \frac{1+\alpha}{4} - \frac{1}{4}\Big[(1+\alpha)^2 - 4\alpha\beta\Big]^{\frac{1}{2}} \tag{2.37}$$

The lower curve corresponds to the symmetric solution (2.24),

$$s = \frac{\alpha\beta}{\alpha+\beta} \tag{2.38}$$

As one can see from figure 6, below $\beta_{\rm crit}$ the data converge to the values of $s$ given by equation (2.37) and above $\beta_{\rm crit}$ to the values of $s$ given by equation (2.38). This is very interesting because it means that fluctuations turn the unstable solution into a stable one and one obtains a first-order phase transition. The best estimate for $\beta_{\rm crit}$ comes from the "fixed point" seen in figure 6, one gets $\beta_{\rm crit} = 0.275 \pm 0.001$ for $\alpha = 1$. By the same method but not

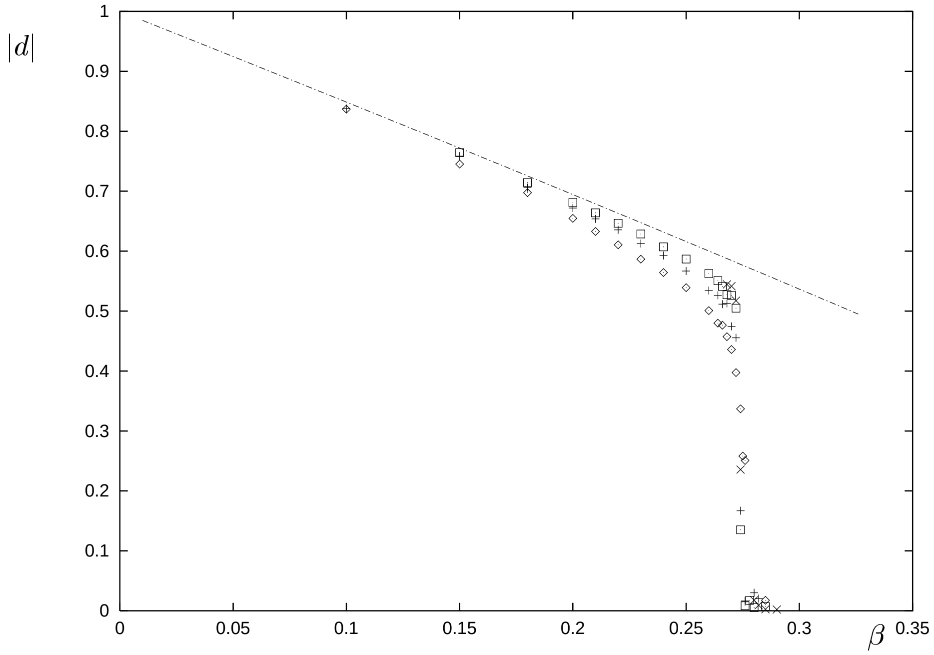


**Figure 5.** Minima of $f_L(d)$ for $L = 100(\diamond), 200(+), 400(\Box), 600(\times)$ sites. The dashed curve gives the mean-field prediction obtained from equation (2.30).

**Table 1.** The critical points for various $\alpha$.

| $\alpha$ | $\beta_{\rm crit}$ | $\alpha$ | $\beta_{\rm crit}$ |
|---|---|---|---|
| 0.25 | 0.1865(5) | 1.25 | 0.269(1) |
| 0.50 | 0.259(1) | 1.50 | 0.264(1) |
| 0.75 | 0.274(1) | 1.75 | 0.258(2) |
| 1.00 | 0.275(1) | 2.00 | 0.253(1) |

with the same patience we have computed the values of $\beta_{\rm crit}$ for other values of $\alpha$. The values are given in table 1.

In the correct phase diagram (figure 7) which replaces figure 1 one has only three regions: the power-law phase ($\tilde{\rm A}$) like in figure 1, the symmetric low-density phase ($\tilde{\rm B}$) (the unbroken phase) which extends down to the diamond-line in figure 1 and finally the domain $\tilde{\rm D}$ under the diamond-line (see figure 7). We have not checked if the separation between the $\tilde{\rm A}$ and $\tilde{\rm B}$ phases is properly given by mean-field but we believe this to be the case because of the analytical calculation on the $\beta = 1$ line done in [24].

A final test of our picture can be obtained looking at the spectrum of the Hamiltonian, which is explicitly given in equation (2.6). We consider the first three levels and take $\alpha = 1$ only. Since the ground state has energy zero, the values of the energies of the next two levels, denoted by $E_1$ and $E_2$, coincide with the energy gaps. If our picture is correct $E_1$ should vanish for large values of $L$ for $\beta < \beta_{\rm crit}$ since in the large $L$ limit one needs two states, the ground state and the first excited state, to describe the two vacua. $E_2$ should be finite. For

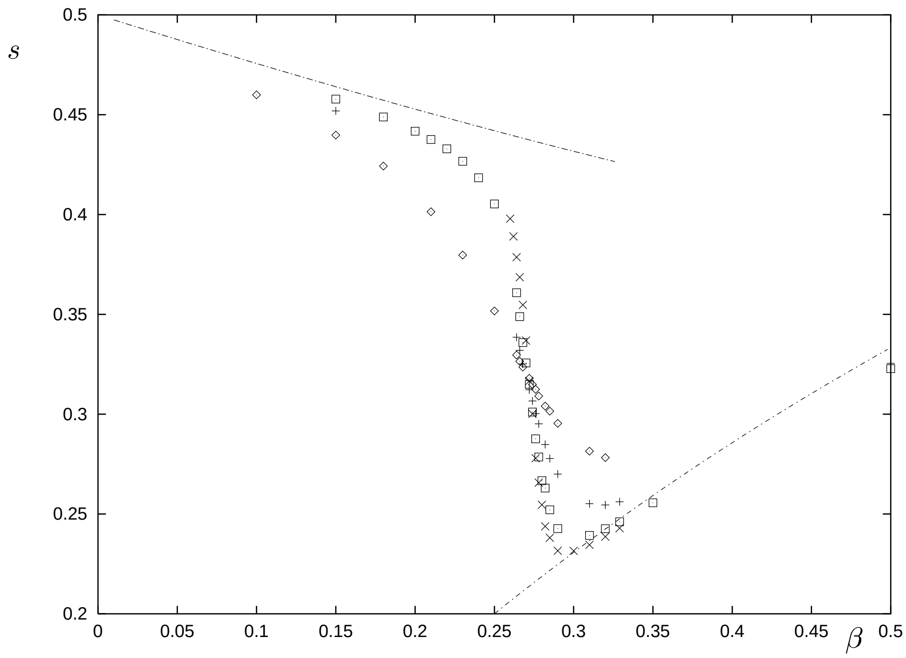


**Figure 6.** Minima of $f_L(s)$ $(s = (p+m)/2)$ as a function of $\beta$ for $L = 100(\diamond), 200(+), 400(\Box), 600(\times)$ sites. The upper curve corresponds to equation (2.37) (broken phases), the lower one to equation (2.38) (unbroken phase).

$\beta > \beta_{\rm crit}$ both $E_1$ and $E_2$ should be finite. Using the modified Arnoldi algorithm of [39] we have calculated, for various values of $\beta$ and chain lengths (up to $L = 11$) the values of $E_1$ and $E_2$. In order to get their large $L$ limit we have used Bulirsch-Stoer approximants [40]. The results are shown in figure 8 which confirms the existence of a critical point around $\beta = 0.275$. If one takes $\beta = \beta_{\rm crit}$ one can estimate the dynamical critical exponent $z$ defined as follows:

$$\lim_{L\to\infty} L^z E_1(L) = \text{const.} > 0 \tag{2.39}$$

where $E_1(L)$ represents the energy of the first exited state for a chain of length $L$. We find $z = 2.0 \pm 0.1$ and therefore a quadratic dispersion relation of a diffusive process.

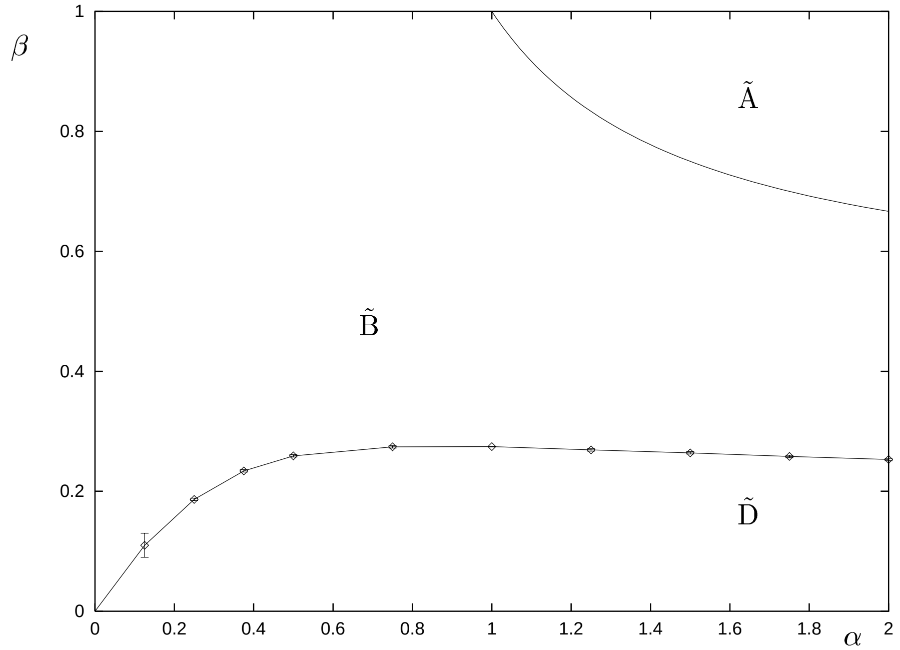


**Figure 7.** Phase diagram of the two-species model for $h = 0$ obtained from the Monte Carlo simulations. The phase $\tilde{\mathrm{A}}$ is given by mean-field approximation.

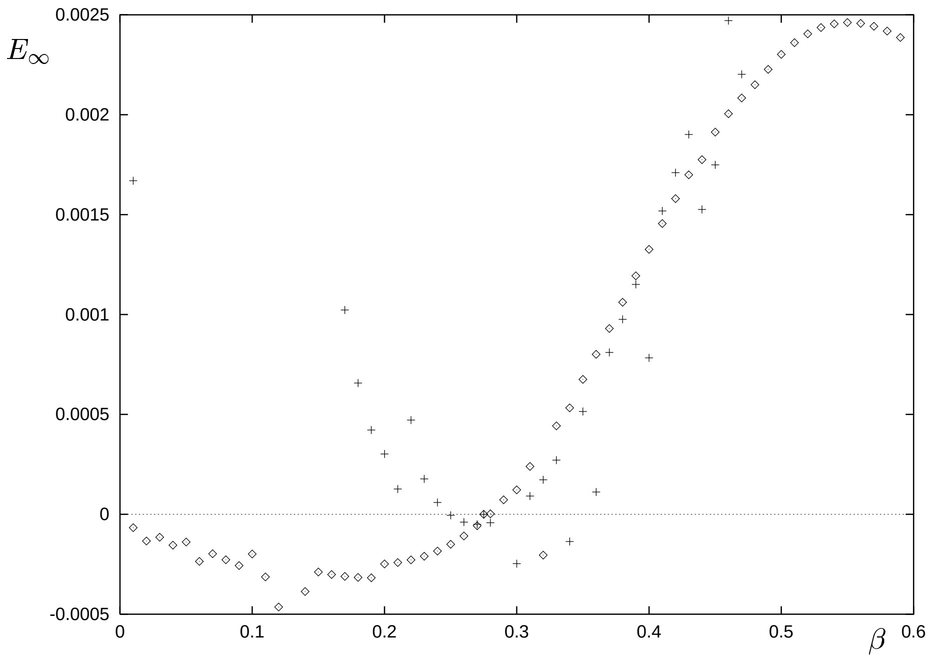


**Figure 8.** Estimates of the first ($\diamond$) and second ($+$) excitations of the $CP$-symmetric Hamiltonian (equation (2.6) with $h = 0$). The estimates were obtained using the spectra of the Hamiltonian up to eleven sites and extrapolating the results in standard ways. Since all eigenvalues of $H$ are positive the errors of the values shown are estimated to be 0.0003.

*2.3. Description of the first-order phase transition*

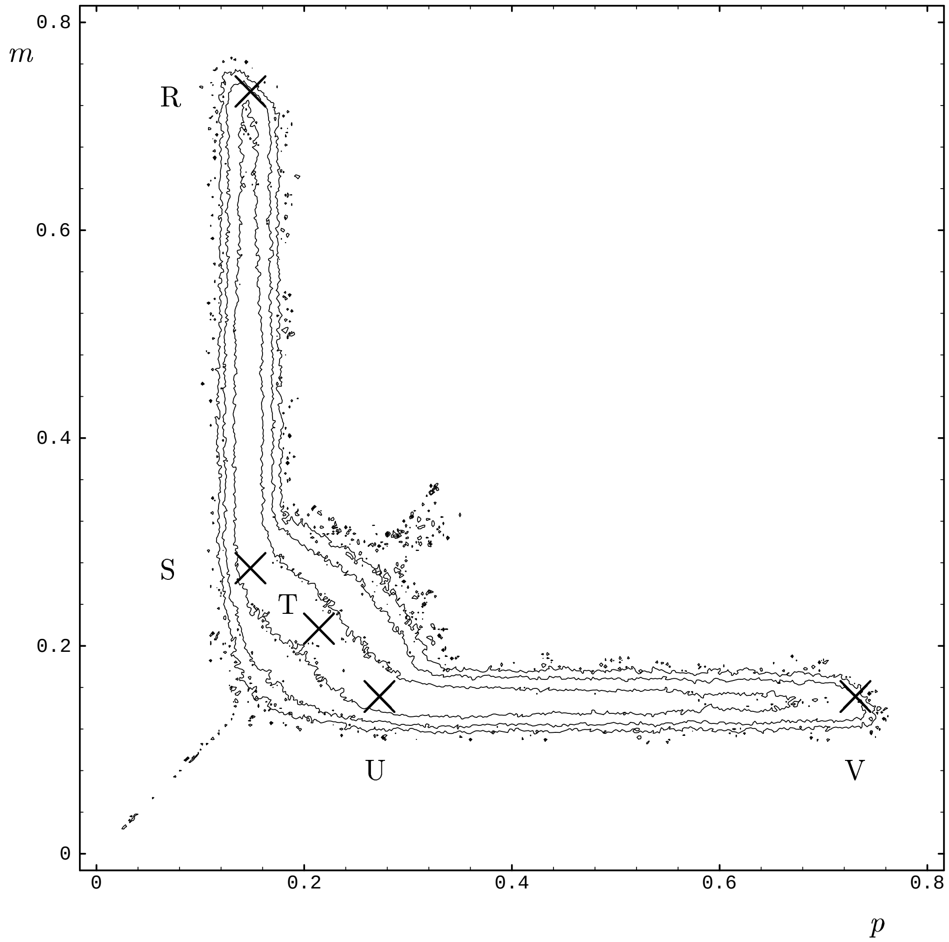


**Figure 9.** Contour lines of $f_L(p,m)$ for $\beta = 0.275$ and $L = 1000$ sites. The "height" difference between lines is constant.

We are now going to study in detail the point $\alpha = 1$, $\beta = \beta_{\rm crit} = 0.275$ where as explained in the last section we have seen a first-order phase transition. The physics of the steady state can be understood only if one considers the two order parameters $p$ and $m$. It is analogously defined to previous defined FEF (see equation (2.8)) and shows the same finite-size behaviour.

In figure 9 we show, in the $p$-$m$ plane, the contour lines of the FEF $f_L(p,m)$ near its minima. The figure suggests a large $L$ limit in which we get the following picture: one line segment parallel to the $p$-axis (from U to V in figure 9), one line segment parallel to the $m$-axis (from S to R), a smooth curve joining the points S, T and U. Let us give the $(p,m)$ coordinates of these five points: V=(0.725,0.149) where $p$ and $m$ are obtained from the mean-field equation (2.30), R=(0.149,0.725), obtained from equation (2.30) exchanging $p$ and $m$, T=(0.216,0.216), obtained from equation (2.24). It is convenient to denote by $p_{\rm V}$ and $m_{\rm V}$ the $p$ and $m$ coordinates of the point V. With this notation the coordinates of the points U and S are due to the *CP* symmetry U=$(1 - p_{\rm V}, m_{\rm V})$ and S=$(p_{\rm R}, 1 - m_{\rm R})$. The points V and

R are to be expected to play a special role since they represent the broken phase for a value of $\beta$ slightly smaller than $\beta_{\rm crit}$. Also the point T is to be expected since it corresponds to the symmetric phase ($\beta$ slightly higher than $\beta_{\rm crit}$). The points S and U are unexpected since they do not correspond to any phase. Their coordinates have however a remarkable property: $p_{\rm U} = 1 - p_{\rm V}$ and similarly $m_{\rm S} = 1 - m_{\rm R}$. These relations are typical for shocks [33].

The following simple model captures the physics of the phase transition. First let us introduce the scaling variable $z = k/L$, where $k$ is the site variable and $L$ the length of the chain. The model will apply in the limit where $k$ and $L$ are large. We assume that the following processes take place:

- With a probability $P_1$ we have shocks of uncorrelated positive particles as described by figure 10a. The probability to find a positive particle at the left of the point $g$ with a density $p_{\rm U}$ and to the right of the point $g$ with a density $p_{\rm V}$ is independent of $z$. One has fronts for $0 < g < 1$ with equal probability (this corresponds to the U-V line segment). The negative particles are also uncorrelated and have a constant density $m_{\rm V}$.
- Also with a probability $P_1$ we have shocks of negative particles (see figure 10b) which are just the *CP*-reflected shocks of the positive particles (this corresponds to the R-S line segment).
- With a probability $P_2$ we have configurations (figure 10c) of constant density (independent of $z$) corresponding to all pairs of values $p$ and $m$ along the line segment S-U, all with the same probability.

Obviously

$$2P_1 + P_2 = 1. \tag{2.40}$$

The assumption that we have a line segment between S and U is an approximation since this line segment intersects the $p = m$ line in the point of coordinates $((p_{\rm U} + p_{\rm R})/2, (m_{\rm S} + m_{\rm V})/2)$=(0.212, 0.212) which does not coincide with T but is very close to it. We did not try to find a better description of the S-T-U curve because this would imply many more Monte Carlo data than we were able to collect.

The probabilities $P_1$ and $P_2$ are determined from the condition that $f_L(p, m)$ has the same value everywhere on the "boomerang". We get for $\alpha = 1$ and $\beta = \beta_{\rm crit}$

$$P_1 = \frac{p_{\rm V} - p_{\rm U}}{2(p_{\rm V} - m_{\rm V})} = 0.39\,, \qquad P_2 = \frac{p_{\rm U} - m_{\rm V}}{p_{\rm V} - m_{\rm V}} = 0.22\,. \tag{2.41}$$

Let us now check the model, in this way we can present the data in an organized way. First, we can can compute $f(d)$. One obtains a function which is flat between $-(p_{\rm V} - m_{\rm V})$ and $(p_{\rm V} - m_{\rm V})$. This is just what one sees in figure 3 for $\beta_{\rm crit}$. Next we compute $m(z)$ and get

$$\begin{aligned} m(z) &= P_1/, m_{\rm V} + \frac{1}{2}P_2(m_{\rm V} + m_{\rm S}) + P_1(m_{\rm R} - z(m_{\rm R} - m_{\rm S})) \\ &= 0.387 - 0.175\, z\,. \end{aligned} \tag{2.42}$$

Obviously $p(z) = m(1 - z)$. In figure 11 we show the density of negative particles as a function of $z$ for various numbers of sites. One notices that the straight line given by equation (2.42) fits the data.

In order to make sure that the linear density distribution observed in figure 11 is not a finite-size effect, in figure 12 we show for $\beta = 0.26$ (below the critical point) the function $m(z)$. One observes that the data converge (slowly) from below to the mean-field value $m = 0.44$ obtained taking the average of the two equations (2.30).

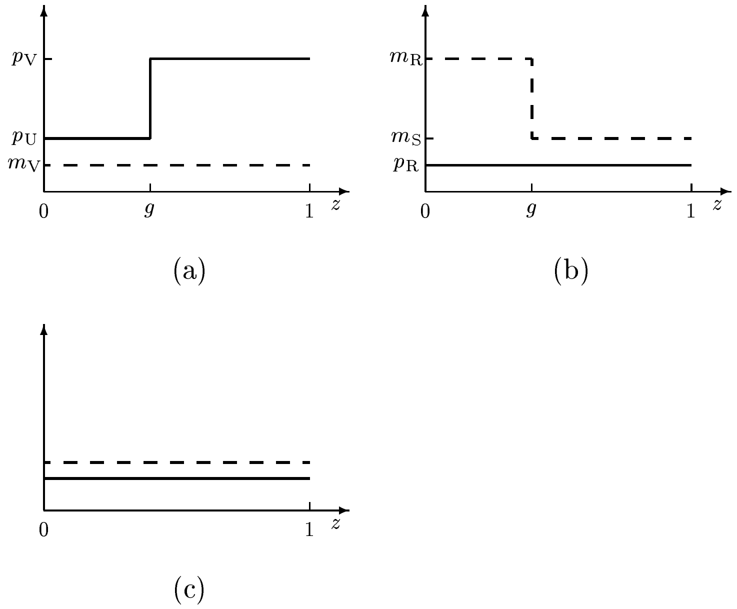


**Figure 10.** The shocks appearing at the first-order phase transition. The solid and the broken lines give the profile of positive and negative particles, respectively.

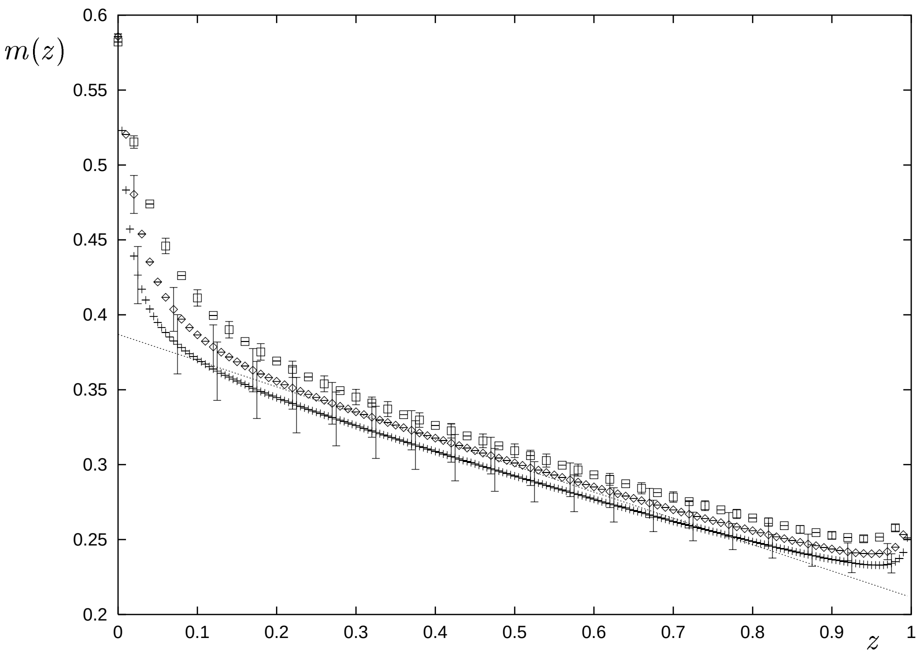


**Figure 11.** Density profile of the negative particles for $L = 50(\square), 100(\diamond), 200(+)$ at the phase transition $\beta = 0.275$. The straight line is given by equation (2.42).

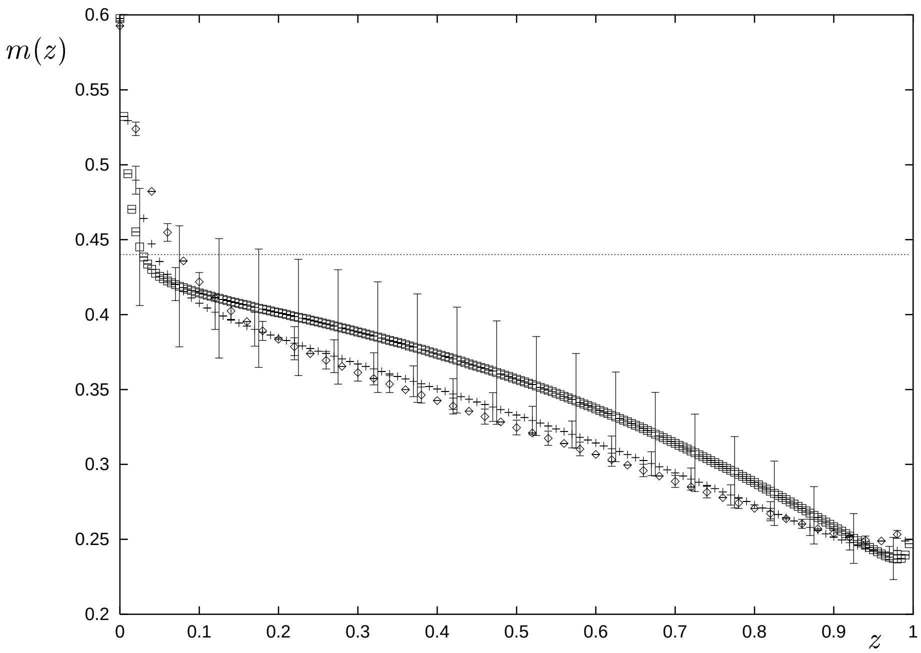


**Figure 12.** Density profile of the negative particles for $L = 50(\diamond), 100(+), 200(\Box)$ at $\beta = 0.26$, below the phase transition. The line gives the mean-field prediction, i.e. the average of the densities of equation (2.30).

In figure 13 we show $m(z)$ for $\beta = 0.3$ (above $\beta_{\mathrm{crit}}$). The data converge from above to the value $m = 0.23$ which is obtained from equation (2.24). In conclusion, the non-constant distributions seen just below and just above $\beta_{\mathrm{crit}}$ are cross-over phenomena.

In order to "see" the shocks, we have looked at configurations where the density of positive particles $p$, averaged over the whole chain, is fixed. This corresponds to a point on the U-V line segment in figure 9 and one expects to see a shock like in figure 10a. Since we are also interested to see what kind of finite-size effects exist, we have chosen to present the densities as functions not of $z$ but in terms of the variable

$$y = \frac{k - k_0}{\sqrt{L}} \tag{2.43}$$

where $k_0$ is the position of the front which in the large $L$ limit is given by

$$k_0 = \frac{L}{2\beta_{\mathrm{crit}} - 1}(p - 1 + \beta_{\mathrm{crit}}). \tag{2.44}$$

The data for $p = 0.5$ are shown in figure 14. Let us leave aside for a moment the existence of "tails" on the left hand side of the figure. The data scale, they are independent of $L$. A good fit to the data is given by

$$p(y) = (\frac{1}{2} - \beta_{\mathrm{crit}})\,\mathrm{erf}(y/2) + \frac{1}{2} \tag{2.45}$$

Obviously, if we show the data as a function of $z$ one gets the front from figure 10a with $g = 0.5$. The value of $m$ in figure 14 corresponds to the value of $m_{\mathrm{V}}$ in figure 10a as expected.

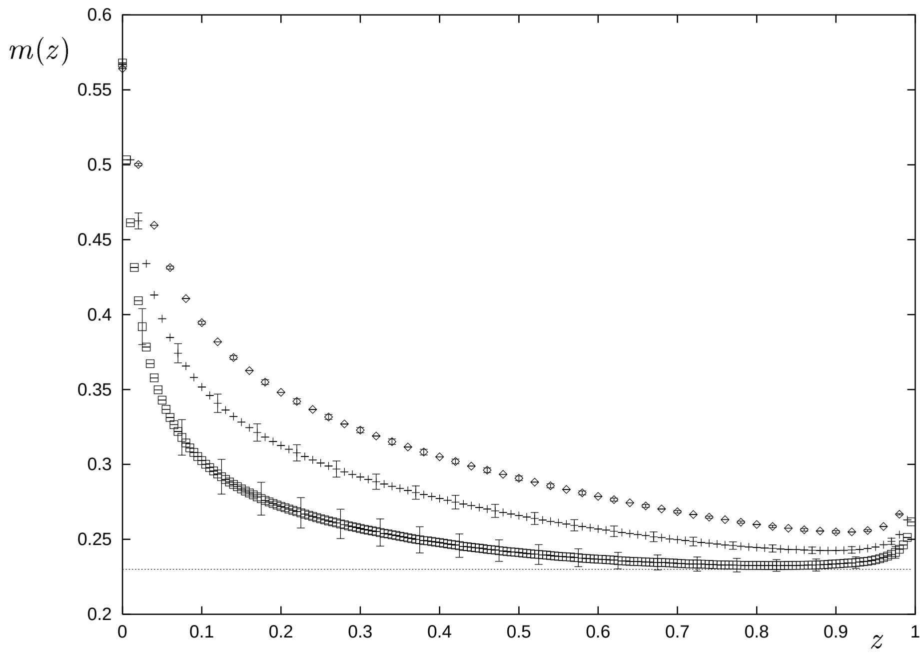


**Figure 13.** Density profile of the negative particles for $L = 50(\diamond), 100(+), 200(\square)$ at $\beta = 0.30$, above the phase transition. The line gives the mean-field solution (2.24).

We now turn our attention to the "tails". For the positive particles one can fit the data like

$$p(k) = \mu\, k^{-\frac{1}{2}} + \beta_{\text{crit}} \tag{2.46}$$

where $k$ is the position of the site starting with the left hand side of the chain and $\mu = 0.08$ is a constant. We have checked that for other shocks (one takes $p$ different of 0.5 but still on the U-V segment in figure 9) the value of $\mu$ stays unchanged. For negative particles the tails are exponential with a correlation length independent of $L$. This observation is intriguing because common sense would suggest that in this case one should have a finite correlation length also in the time direction, i.e. masses in the spectrum of the problem and not only the massless excitations discussed in previous section.

Another test of the model, this time on a part of it on which we certainly expect to be less precise, is to "cut" through the handle of the boomerang. We have taken $d = 0.05$ in order to check if profiles like in figure 10c are seen. The data are shown in figure 15 together with the expected constant values (take the intersection of the line $d = 0.05$ with the line segment S-U in figure 9). As one notices we find agreement. After presenting the data we are left with a puzzle. We have expected the point T to be singled out in some way (it represents the symmetric phase), but it is not.

### *2.4. The broken phases in the presence of a symmetry breaking external source*

As explained in section 2.1 and shown in figure 7, the phase diagram of the $CP$-symmetric model consists of a power-law phase $\tilde{\mathrm{A}}$ and a broken phases $\tilde{\mathrm{D}}$ separated by a first-order phase transition line from the unbroken phase $\tilde{\mathrm{B}}$. In equilibrium systems, if one has a transition from

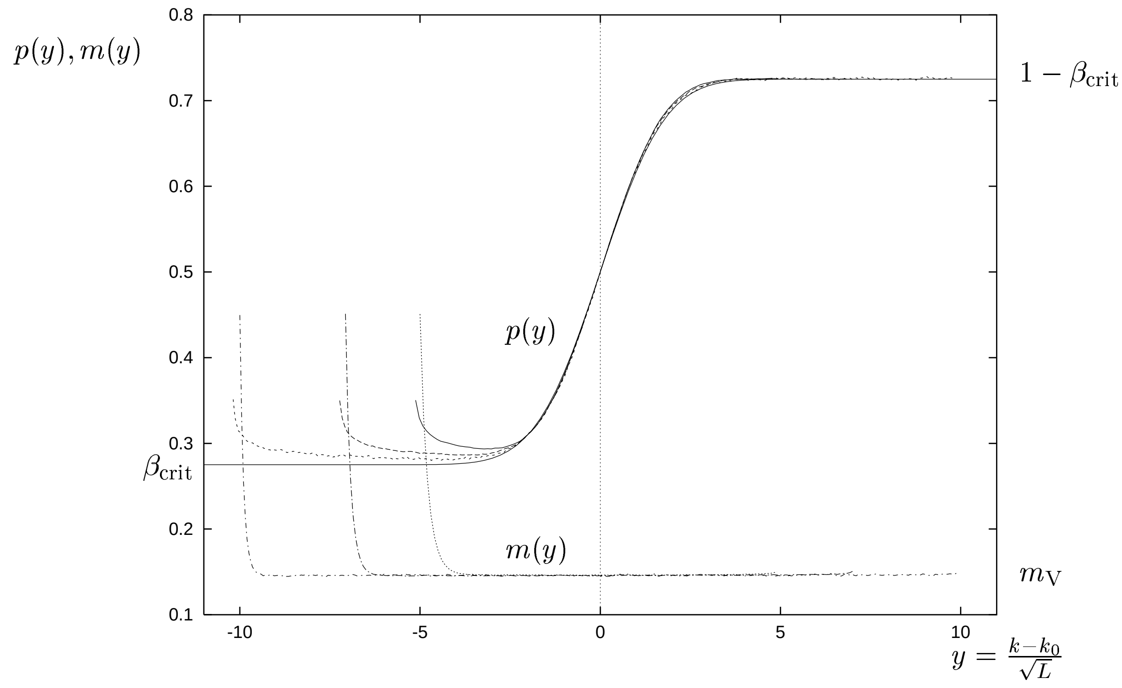


**Figure 14.** Scaling of the shock: Density profiles of positive and negative particles for $p = 0.5$ fixed. Data for $L$ =100, 200, 400 sites. The solid curve fitted to the shock is given by equation (2.45). Equation (2.44) gives the expression of $k_0$.

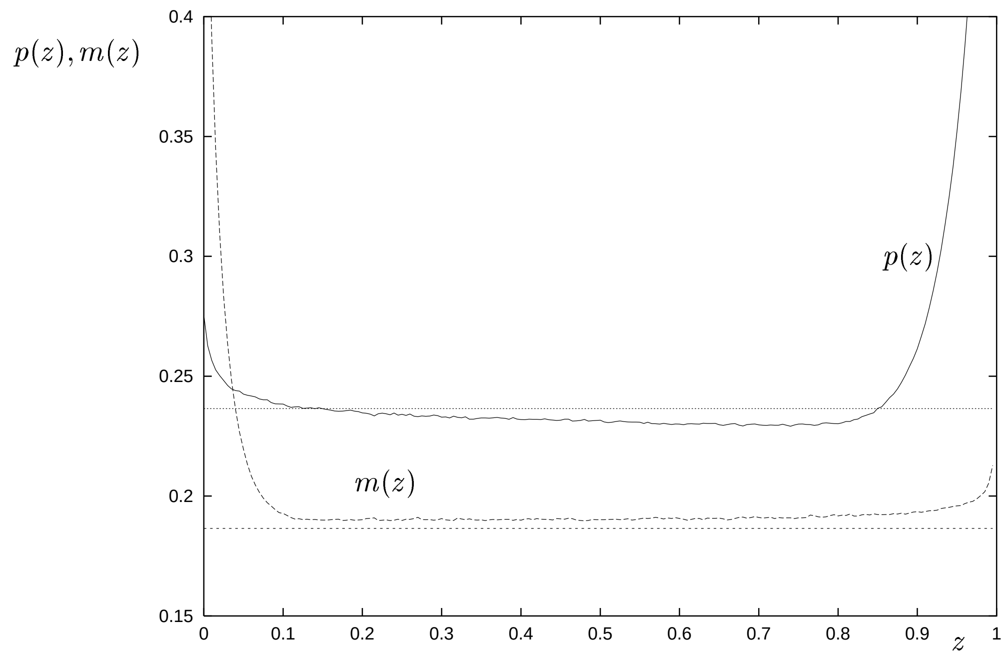


**Figure 15.** Density profile $p(z)$ and $m(z)$ for $d = 0.05$ and $L = 200$.

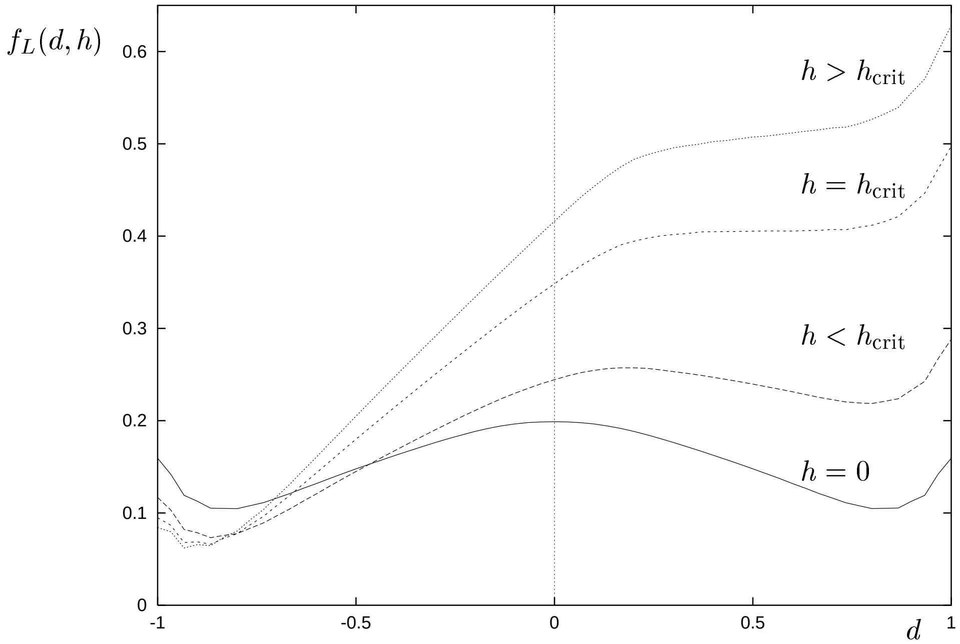


**Figure 16.** $f_L(d,h)$ for $L = 30$, $\alpha = 1.0$, $\beta = 0.1$ and $h = 0$, 0.1, 0.2281, 0.3. For $h = 0$ the system is in the phase $\tilde{\mathrm{D}}$.

an ordered to a disordered phase, the broken phase corresponds to first-order phase transitions (and the FEF is a flat function between the two phases). As we have seen this is not the case for steady states and for this reason we use the expression "first-order" only on the separation line where the FEF is flat and the expression "broken phase" for the domain where the FEF is not convex and has two minima.

We consider now the effect of an explicit *CP* symmetry breaking in the model. We take $h > 0$ in the boundary rates given by equations (2.2) and (2.3). Using Monte Carlo simulations, we have computed the FEF $f_L(d,h)$ taking $\alpha = 1$ and several values of $\beta$ and $h$; $d$ is again the difference between the average densities of positive and negative particles. In figure 16 we show $f_L(d,h)$ for $\beta = 0.1$ (in the $\tilde{\mathrm{D}}$ region in figure 7) and several values of $h$. As expected the FEF is symmetric for $h = 0$ and gets asymmetric for $h > 0$. We observe that below $h_{\mathrm{crit}} = 0.2281$ the FEF shows two minima and only one minimum for $h > h_{\mathrm{crit}}$. For $h = h_{\mathrm{crit}}$ the first and second derivative of $f_L(d,h)$ with respect to $d$ vanishes. This is the definition of a spinodal point [36].

The behavior of $f_L(d,h)$ is the one expected from a Ginzburg-Landau ansatz [31]. Our data are of course not precise enough to give an estimate with four digits for $h_{\mathrm{crit}}$, the value we give is obtained in the mean-field approximation. We will return soon to the problem of the validity of mean-field.

In the Ginzburg-Landau ansatz $f(d,h)$ has a simple $h$ dependence:

$$f(d,h) = f(d,h=0) + \nu\, h\, d + g(h) \tag{2.47}$$

where $\nu$ is a parameter. We have collected data for various values of $\beta$ and $h$ and find $\nu = 1.4$ getting a fit to the data within 10%. In figure 17 we fix the value of $h = 0.02$ and show the

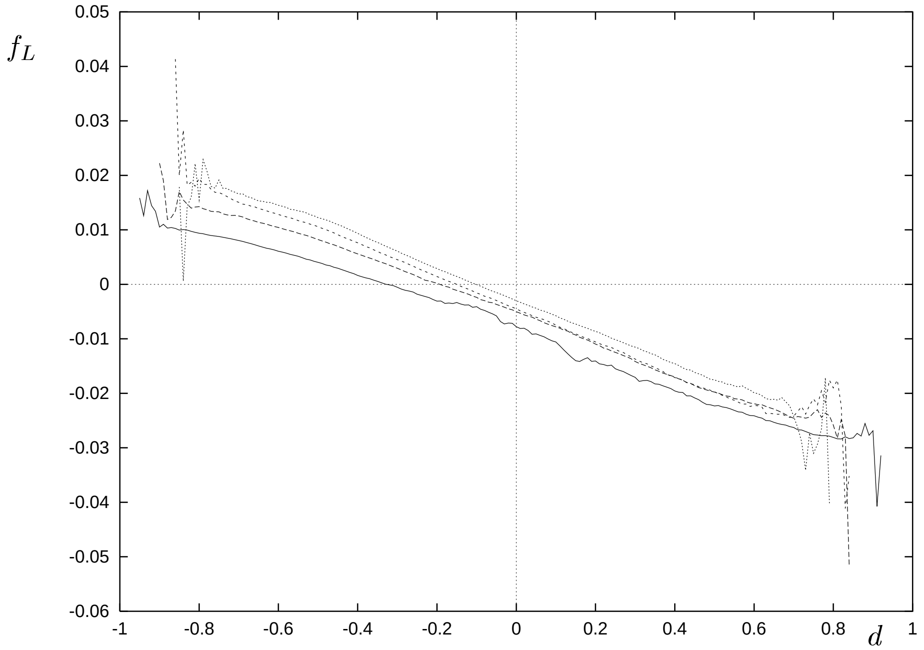


**Figure 17.** $f_L(d, h = 0) - f_L(d, h = 0.02)$ for $\beta$ =0.20, 0.26, 0.28, 0.30 and $L = 100$ sites.

difference

$$f_L(d, h = 0) - f_L(d, h = 0.02) \tag{2.48}$$

as a function of $d$. According to equation (2.47) we expect straight lines with the slope $-0.028$. The data are compatible with this prediction. We have repeated the simulations for several values of $h$ with the same result.

In section 2.1 we have computed the mean-field approximation of the model for $h$ greater than zero, extending the calculation done in [24]. Like in the $h = 0$ case, we want to understand in a simple way where and in which way mean-field is exact or wrong. In table 2, for different values of $\beta$ and $h$, we give the values of $d_L^{\text{min}}$ which denotes the minima of the FEF as determined by Monte Carlo simulations as well as the values of $d_{\text{mf}}$ obtained in mean-field. Comparing the Monte-Carlo simulations with the mean-field results we reach the conclusion that probably mean-field is not exact anywhere. It is however a good approximation for small values of $\beta$ and large values of $h$.

We are now going to discuss some aspects of the dynamics of the model when one includes the symmetry breaking term. In figure 18 we give the energies of the first excited state for various $h$. Our attention goes first to the spinodal point, $h_{\text{crit}}$, and we look at the spectrum of the Hamiltonian (2.6). We notice that the first excited state has an energy which vanishes in the large $L$ limit. The dynamical critical exponent (see equation (2.39)) determined using the values of the first excited state of chains up to 11 sites $\beta = 0.1$ and $h_{\text{crit}} = 0.22810$ as given by mean-field is $z = 1.00 \pm 0.01$. We have repeated the same calculation for $\beta = 0.05$ ($h_{\text{crit}} = 0.28096$) and found $z = 1.000 \pm 0.001$. As discussed previously, it is not clear if the values of $h_{\text{crit}}$ obtained by mean-field can be trusted to a precision of five digits. To our knowledge it is for the first time that the exponent $z = 1$ appears in stochastic processes.

**Table 2.** The minima $d_L^{\mathrm{min}}$ of $f_L(d)$ (error $\pm 0.01$) and the mean-field predictions $d_{\mathrm{mf}}$ for $\alpha = 1$, various $\beta$ and $h$. Values of $d_L^{\mathrm{min}}$ predicted (within 10%) are printed bold face. Several values given for a set of parameters $\alpha$, $\beta$, $h$ reflect different minima ($d_L^{\mathrm{min}}$) or different stationary solutions of the mean-field equations ($d_{\mathrm{mf}}$).

| $\beta$ | $h$ | $L$ | $d_L^{\mathrm{min}}$ | $d_{\mathrm{mf}}$ |
|---|---|---|---|---|
| 0.6 | 0 | 200 | **0.00** | 0 |
| | 0.1 | 200 | **-0.08** | -0.0943 |
| 0.35 | 0 | 400 | **0.00** | 0 |
| | 0.02 | 100 | -0.05 | -0.468 |
| | 0.1 | 100 | -0.45 | -0.512 |
| 0.329 | 0 | 400 | 0.00 | -0.490/+0.490/0 |
| | 0.02 | 200 | -0.06 | -0.501 |
| | 0.1 | 200 | **-0.52** | -0.543 |
| 0.3 | 0 | 400 | 0.00 | -0.537/+0.537/0 |
| | 0.02 | 400 | -0.15 | -0.546/+0.527/+0.098 |
| | 0.1 | 400 | **-0.58** | -0.584 |
| 0.26 | 0 | 200 | **-0.53/+0.53** | -0.600/+0.600/0 |
| | 0.01 | 100 | **-0.53**/+0.43 | -0.604/+0.596/+0.019 |
| | 0.02 | 100 | **-0.54** | -0.607/+0.592/+0.038 |
| | 0.07 | 100 | **-0.61** | -0.629 |
| 0.1 | 0 | 200 | **-0.84/+0.84** | -0.849/+0.849/0 |
| | 0.02 | 100 | **-0.84/+0.84** | -0.852/+0.846/+0.00519 |
| | 0.05 | 100 | **-0.85/+0.83** | -0.856/+0.841/+0.013 |
| | 0.1 | 50 | **-0.86/+0.81** | -0.864/+0.833/+0.026 |

We would like to make another observation on the flip times related to barriers in the FEF. Let us take $\beta = 0.1$ and $h = 0.1$ in figure 16 and denote by $\Delta_1$ ($\Delta_2$) the difference between the maximum of the FEF and the minimum of the FEF for negative (positive) values of $d$ ($\Delta_2 = 0$ at the spinodal point). From the Monte Carlo data ($L = 50$ sites) we get $\Delta_1 = 0.178 \pm 0.002$ and $\Delta_2 = 0.041 \pm 0.002$. The two flip times from the stable (meta-stable) to the meta-stable (stable) phase are $T_{\mathrm{long}}$ ($T_{\mathrm{short}}$). They have been measured for chains of different lengths $L$ and their values are shown in figure 19. They both increase exponentially with the system size, therefore we call the phase in the absolute minimum stable and the other one meta-stable. In principle, we can only at this point establish spontaneous symmetry breaking for the *CP*-invariant case $h = 0$, since the flip times increase exponentially as the dimensionality of the configuration space. The straight lines in figure 19 are given by the ansatz

$$\begin{aligned} T_{\mathrm{long}} &\propto \exp(\Delta_1\, L) \\ T_{\mathrm{short}} &\propto \exp(\Delta_2\, L)\ . \end{aligned} \tag{2.49}$$

The agreement between the ansatz (2.49) and the data shows a connection between the dynamics of the model (flip times) and the properties of the steady state (the FEF). Repeating the same procedure for a different value of $\beta$ gives the same result.

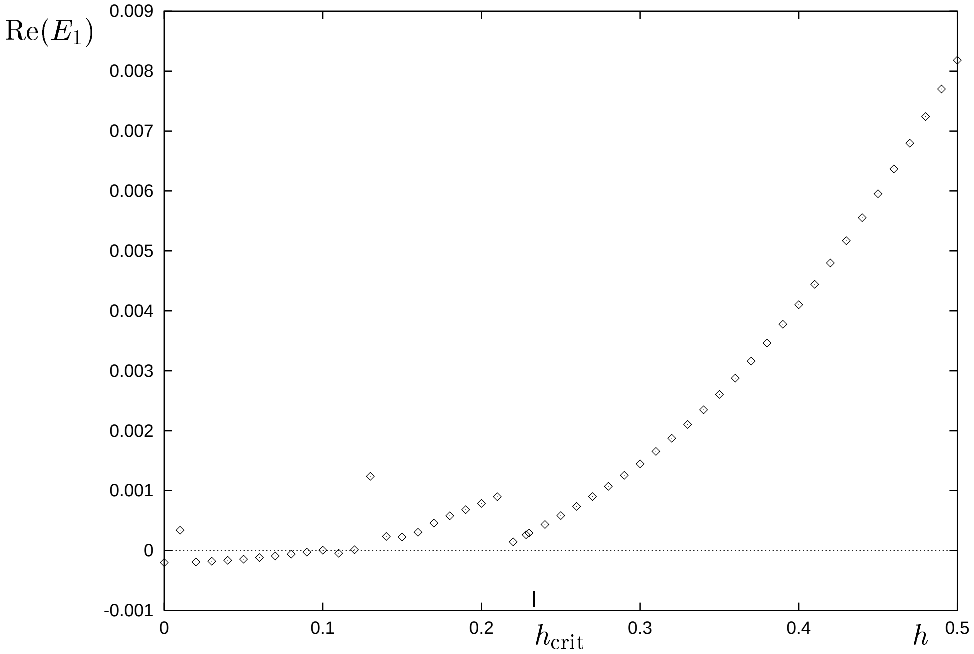


**Figure 18.** Estimates of the first excitation of the Hamiltonian (equation (2.5) in an external field $h$. The estimates were obtained using the spectra of the Hamiltonian up to eleven sites and extrapolating the results in standard ways. Since all eigenvalues of $H$ are positive the errors of the values shown are estimated to be 0.0003.

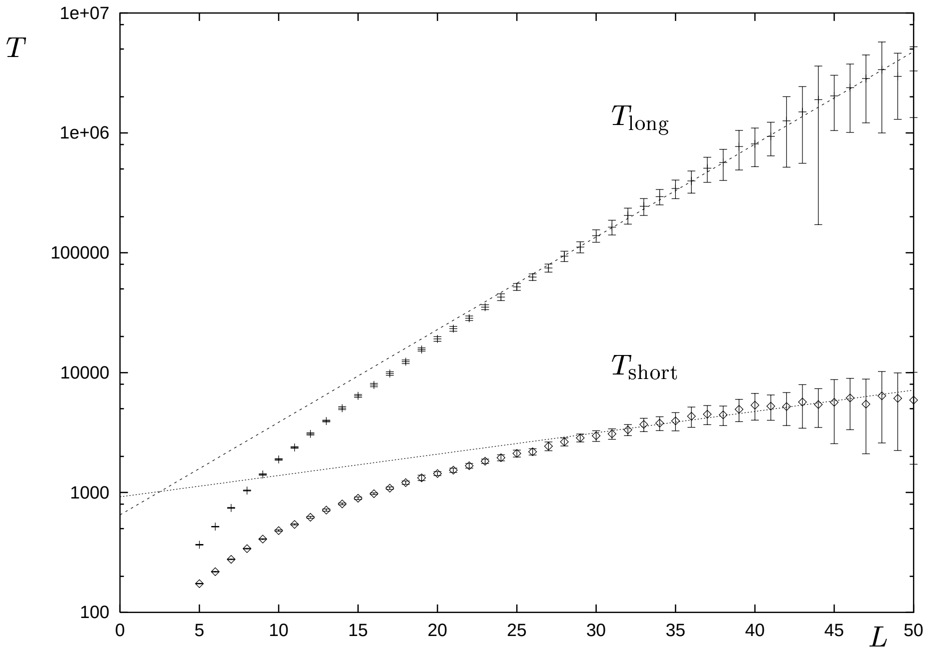


**Figure 19.** Logarithmic plot of the flip times for $\alpha = 1.0$, $\beta = 0.1$ and $h = 0.1$. The dotted curves are given by equation (2.49).

## 3. The RWT model

The aim of this chapter is to introduce a simplified version of the above three-state diffusion model which still captures spontaneous symmetry breaking and in which one can study spinodal points.

To do so, let us consider the model defined by the processes (2.1)–(2.3) in the limit output $\beta \to 0$ [37]. The time scale is then determined by the output rate $\beta$, and we therefore introduce a rescaled time $\tau = 2\beta t$. In the limit the relevant configurations are those composed of three blocks, with $j$ negative particles to the left, $v$ vacancies in the middle and $k$ positive particles on the right, with $L = j + v + k$,

$$(j,k) \;=\; \underbrace{(-)\cdots(-)}_{j}\,\underbrace{(\,0\,)\cdots(\,0\,)}_{v}\,\underbrace{(+)\cdots(+)}_{k}\,. \tag{3.1}$$

All other configurations may be neglected. Since the output is small, any configuration different from those above will quickly (in the $\tau$ time scale) rearrange itself until all particles are waiting to exit.

Suppose now a particle leaves the system. Either it will be replaced by a particle of the opposite sign, which will quickly traverse through the system to join the block of particles of the same sign, or the hole thus created will itself travel through the system to join the block of holes. On the $\tau$ time scale the system involves transitions between various three-block configurations (3.1). Note, that if the last particle of its type leaves the system, then particles of the other type will quickly fill up the system, before again one of the these particles leaves the system. Hence we have to take the configurations $(j,k)$ in

$$T_L = \{(j,k) \mid j,k \text{ integers } > 0 \text{ with } j+k \leq L\}$$

into account.

Let us now give a quantitative description of the dynamics in the configuration space. Consider now what happens during a time interval $\mathrm{d}\tau$ which is short on the $\tau$ time scale but long on the $t$ time scale. We ignore the possibility that more than one particle may exit in such an interval. There is a small probability $\mathrm{d}\tau(1-h)/2 = \beta(1-h)\mathrm{d}t$ that a negative particle at site 1 leaves the system during that interval. Suppose that happens.

(i) If $j > 1$, then either the hole thus created is filled by the positive particle, or the negative particle on site 2 exchanges position with the hole. The relative probabilities of these processes are $\alpha/(1+\alpha)$ and $1/(1+\alpha)$. Either event will be followed by a rearranging of the particles, resulting in configuration $(j-1, k+1)$ or $(j-1, k)$.

(ii) If $j = 1$, then all negative particles have left the system and positive particles will fill up the system quickly, resulting in a configuration $(0, L)$. This configuration can only be followed by the configuration $(1, L-1)$, through an exit of a positive particle. We therefore neglect this last process.

The dynamics of these configurations may be represented by a biased random walk in the triangle $T_L$ The model is therefore called random walker on a triangle (RWT) model.

To summarize, the following processes may take place in a rescaled time interval $\mathrm{d}t$ with probability $p$:

$$(j,k) \to (j-1,k) \qquad \text{if } j > 1 \text{ with } p = a(1+h)\mathrm{d}t$$
$$(j,k) \to (j,k-1) \qquad \text{if } k > 1 \text{ with } p = a(1-h)\mathrm{d}t$$

$$
\begin{aligned}
&(j,k) \to (j-1,k+1) && \text{if } j>1 \text{ with } p=b(1+h)\mathrm{d}t \\
&(j,k) \to (j+1,k-1) && \text{if } k>1 \text{ with } p=b(1-h)\mathrm{d}t \\
&(1,k) \to (1,L-1) && \text{with } p=c(1+h)\mathrm{d}t \\
&(j,1) \to (L-1,1) && \text{with } p=c(1-h)\mathrm{d}t \ .
\end{aligned} \tag{3.2}
$$

Where we introduced the notation

$$
a=\frac{1}{2(1+\alpha)}\,,\qquad b=\frac{\alpha}{2(1+\alpha)}\,,\qquad c=\frac{1}{2} \tag{3.3}
$$

The first four processes in (3.2) are local hops to neighbouring sites on the triangle, the last two are non-local jumps to the corners $(1,L-1)$ and $(L-1,1)$ respectively. For $h=0$ the definitions are invariant under reflection on the line $j=k$ corresponding to the *CP* symmetry of the three-state diffusion model above. (Therefore the reflection symmetry of the RWT model will also be denoted as *CP* symmetry in the following.) We fix the unit of time choosing $c=1/2$. This renders the probability rates dimensionless. It would be interesting to study the general case $a+b\neq 1/2$ as well.

Since the RWT model is the $\beta\to 0$ limit of the three-state diffusion model, and the first-order phase transition occurs in the latter model for finite $\beta$ we might not study the this transition here. But we expect spinodal points to occur. At the spinodal line, the previous investigation suggested $z=1$ for $h\neq 0$. This is the motivation to study time-dependent properties, metastability and spinodal points in more detail with the RWT model. All these are manifestly associated with non-equilibrium models [36].

The time evolution of the RWT model is again given by the master equation [9]

$$
\frac{\mathrm{d}}{\mathrm{d}t}|P>=-H\,|P>\ , \tag{3.4}
$$

where $|P>$ is now the vector of the probabilities $P(j,k)$ of finding the random walker at site $(j,k)$ on the triangle $T_L$. The Hamiltonian $H$ is the time evolution operator and is fully determined by the processes (3.2). The stationary properties of the system are given by the ground state $|P_0>$ with $H\,|P_0>=0$, and the dynamical properties are given by the excitations of $H$.

The configuration space of any many-particle models grows exponentially with the system size in contrast to the configuration space of the RWT model which has dimension $L(L-1)/2$. This polynomial dependence on $L$ enabled us to investigate the spectrum of the model in much greater detail as above. By numerical diagonalization of the Hamiltonian (see the next section), we found an interesting two band structure of the spectrum, which leads to two gaps or time scales. At the spinodal point $h_{\mathrm{crit}}=a/(1-a)$, one scale vanishes with critical exponent $x=2$ and the lower part of the spectrum has the form $E_j=a\,k_j/L$, i.e. we find $z=1$ at the spinodal point in this model as well. The constants $k_j$ are universal, and do not depend on the remaining parameter $a$. This reminds one of the critical spectrum of a quantum spin chain related to a conformal field theory. As a surprise, the imaginary parts of the constants $k_j$ have the form $\mathrm{Im}\,k_j=j\,\mathrm{Im}\,k_1$. For the real parts, we do not find any regularity.

The value of $h_{\mathrm{crit}}$ has already been conjectured in [37]. It is also predicted by taking the $\beta\to 0$ limit of the mean-field results for the three-state model (see equation (2.35)). There, mean-field theory was found to be compatible with simulations for small $\beta$.

Besides the study of the time evolution operator one can investigate the free energy functional (FEF) of the RWT model. This functional $f$ is here defined as:

$$f_L(d) = -\frac{1}{L} \log P_0(d, L) \ , \qquad f(d) = \lim_{L\to\infty} f_L(d) \ , \tag{3.5}$$

where

$$d = (j-k)/L \tag{3.6}$$

is an order parameter, and $P_0(d, L)$ denotes the corresponding stationary probability distribution.

Analogously to the "low-temperature" regime of the three-state model, one finds that the FEF of the RWT model has two global minima ($d = -1, +1$) in the *CP*-symmetric case ($h = 0$). In the limit $L \to \infty$, the symmetry is spontaneously broken and there are two equally stable phases with $d = \pm 1$. For $0 < h < h_{\text{crit}}$, the dynamics (3.2) favours the movement to lower values of the order parameter and the FEF has a global minimum ($d = -1$) and a local minimum ($d = +1$). This leads to the existence of a stable and a meta-stable phase in the infinite volume limit ($L \to \infty$), the random walker staying near the favoured corner F$=(1, L-1)$ and the unfavoured corner U$=(L-1, 1)$ respectively. Above $h_{\text{crit}}$ there exists only one phase, the random walker always staying around F. This is also reflected in the spectrum of the Hamiltonian (3.4), since one has two ground states for $L \to \infty$ and $h < h_{\text{crit}}$ and only one for $h > h_{\text{crit}}$.

It is also possible (see section 3.2) to measure the flip time from one phase to the other using Monte Carlo simulations. At the spinodal point, one observes a discontinuity in the passage time from the corner U to the corner F. At and above $h_{\text{crit}}$, the average time taken to reach the corner F grows linearly with $L$. However, there is a discontinuity in the proportionality constant as one approaches $h_{\text{crit}}$ from above. The linearity above $h_{\text{crit}}$ can be explained by a mean-field argument, the linearity at $h_{\text{crit}}$ cannot. The time taken to reach the corner U and the time taken to reach the corner F for $h < h_{\text{crit}}$ grow exponentially with $L$. These flip times can be connected to masses appearing in the spectrum of the model with additional absorbing configurations. This will be explained in section 3.3.

Using Monte Carlo simulations, one can also investigate the movement of the random walker starting from a specific initial position. Analysing the mean path, one again identifies two time scales away from the spinodal point, and at the spinodal point, one again finds universal behaviour (section 3.4).

All the results found here for the RWT model are in accordance with the results found for the three-state diffusion model (chapter 2). But the detailed analysis of the spectrum of the time evolution operator now suggests a link between the time scales found in the spectrum, the time scales found in the flip times, and the scales one observes in the movement of the random walker. This was not observed before.

### *3.1. The spectrum of the time evolution operator*

The RWT model corresponding to a three-state model of $L$ sites has only $L(L-1)/2$ configurations. Therefore it becomes possible to study the spectrum of its time evolution operator $H$ (2.6) and to extrapolate the finite size data to the large $L$ limit. For the three-state model this could only be done for the first excitation and with a less precise extrapolation from up to 11 sites.

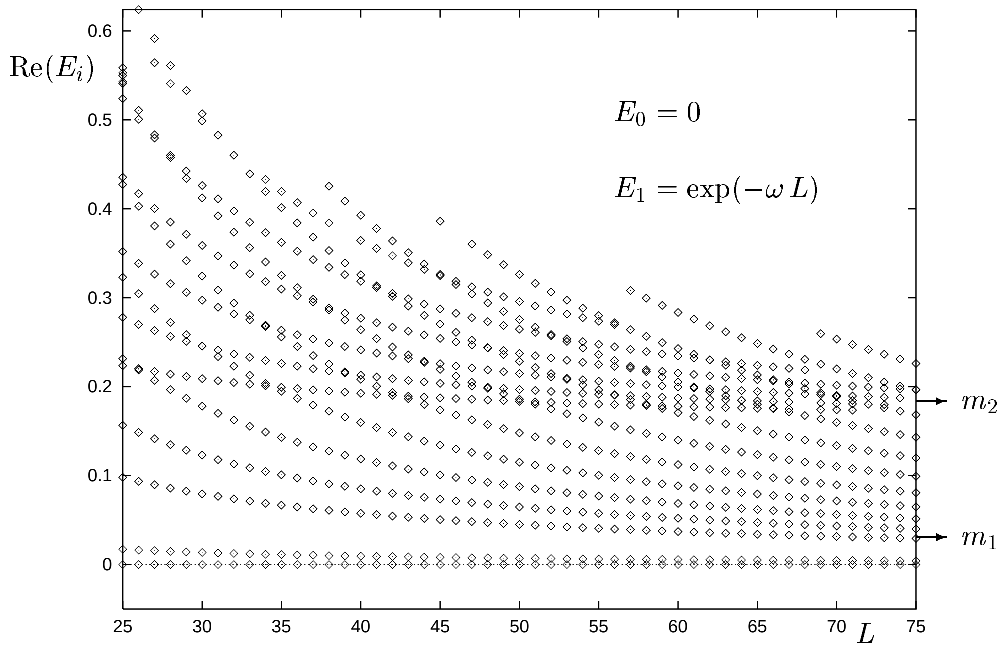


**Figure 20.** Dependence of the spectrum on system size. The data is from numerical diagonalization for $a = 1/4$, $h = 0.3$. Shown are the real parts of the eigenvalues of $H$. The gaps $m_1$ and $m_2$ extrapolate to finite values as seen in figure 21.

Using a modified version of the Arnoldi algorithm [39], we have calculated the low-lying eigenvalues (up to the 30th level) of the time evolution operator $H$ of the RWT model for $L \leq 220$, various values of $h$, and $a = 0.001, 0.1, 0.25, 0.4$. Apart from the ground state "energy" $E_0(L) \equiv 0$, the further eigenvalues of the non-hermitian matrix $H$ are positive, or complex with positive real parts. Since the Hamiltonian matrix has real entries only, complex eigenvalues come in conjugated pairs. Typical results for the real part of the spectrum (for $a = 0.25, h = 0.3$) are shown in figure 20. One identifies two bands of excitations leading to the gaps (time scales) $m_1$ and $m_2$ in the large $L$ limit. Note that the excitations correspond to energy gaps, since the ground state energy of $H$ is zero for any system size. Values for the large $L$ limit were extrapolated from data for finite $L$ using the Bulirsch-Stoer algorithm [40].

The most important observation is that there exists a critical spinodal point at (see figure 21)

$$h_{\text{crit}} = \frac{a}{1-a}\,. \tag{3.7}$$

At this point, the system looses one of its time scales ($m_1 = 0$) and acquires a band of excitations with a universal $L^{-1}$ dependence.

The results for the spectrum of $H$ can be summarized as follows:

- *first excitation:*
  For $h < h_{\text{crit}}$ the first excited energy level approaches zero as
  $$E_1 \propto \exp(-\omega L) \tag{3.8}$$
  This excitation is real, the higher excitations are complex conjugated pairs. Thus, in the

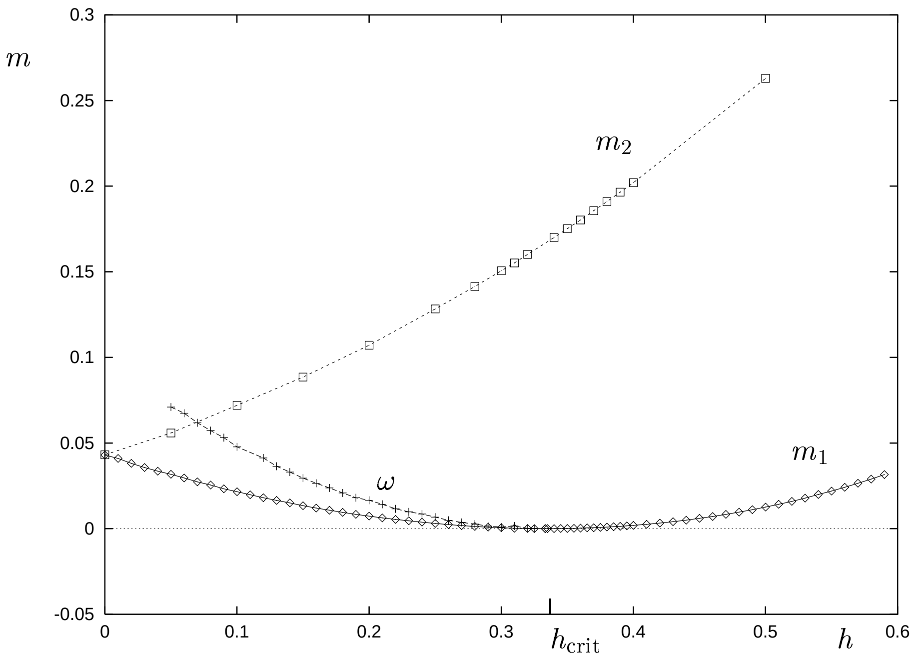


**Figure 21.** Length scale $\omega$, and upper and lower gaps $m_1$ and $m_2$ for $a = 1/4$. The values given are extrapolated from data of numerical diagonalization of $H$ up to $L = 220$.

limit $L \to \infty$, there are two ground states. Linear combinations of the eigenvectors give two phases [35]. For $h = 0$ they are equally stable, while for $h > 0$ one of them is stable, and the other is meta-stable. The two phases correspond to minima of the free energy functional at $d = 1$ and $d = -1$ (see section 3.2). The meta-stable phase vanishes at the spinodal point $h_{\text{crit}}$. Above $h_{\text{crit}}$, there is only one ground state for $L \to \infty$, i.e. none of the excited levels approaches zero.

- *higher excitations:*
  Above $E_0$ and $E_1$, there are two bands of complex eigenvalues of the form
  $$E_j^{(1)}(L) = m_1 + k_j^{(1)}/L + \cdots \tag{3.9}$$
  $$E_j^{(2)}(L) = m_2 + k_j^{(2)}/L + \cdots \quad . \tag{3.10}$$
  The gaps $m_1$ and $m_2$ are real, whereas the constants $k_j^{(i)}$ have imaginary parts, such that one has complex conjugated pairs of eigenvalues. One finds that $m_1$ is proportional to $\omega$. For $a = 0.25$. we find $m_1 = 0.57(4)\ \omega$.
  For $h = 0$ one has $m_1 = m_2$ and the constants $k_j^{(1)} = k_j^{(2)} = k$ are independent of $j$, i.e. the $1/L$ term is the same for all excitations in contrast to equations (3.9) and (3.10) for $h > 0$. There are two ground states (compare equation (3.8)), corresponding to equally stable phases.
  For $h > h_{\text{crit}}$ the excitations again come in the form of two bands as in equations (3.9) and (3.10).

- *lower gap:*

**Table 3.** Excited levels of $H$ at $h_{\rm crit}$: $E_j = a\,k_j/L$. Complex excitations come in conjugated pairs.

| level | $\mathrm{Re}(k_j^{(1)})$ | $\mathrm{Im}(k_j^{(1)})$ | $\mathrm{Im}(k_j^{(1)})/12.81$ |
|---|---|---|---|
| 1 | 1.7080 | 0 | 0 |
| 2 | 8.4980 | 12.7663 | 0.997 |
| 4 | 10.368 | 25.771 | 2.012 |
| 6 | 11.504 | 38.548 | 3.009 |
| 8 | 12.324 | 51.241 | 4.000 |
| 10 | 12.97 | 63.89 | 4.988 |
| 12 | 13.5 | 76.52 | 5.994 |

For $h \to h_{\rm crit}$, the lower gap $m_1$ vanishes, as does $\omega$, which is proportional to $m_1$. For $h < h_{\rm crit}$, the gap is given by $m_1 = \lim_{L\to\infty} E_2(L)$. Above $h_{\rm crit}$, the first excitation does not give a second ground state for $L \to \infty$ and one finds a non-zero gap $m_1 = \lim_{L\to\infty} E_1(L)$. The gap $m_1$ given by

$$\begin{aligned} m_1 &= 0.42(2)\ (h_{\rm crit} - h)^x \quad \text{for } h < h_{\rm crit} \\ m_1 &= 0.46(2)\ (h - h_{\rm crit})^x \quad \text{for } h > h_{\rm crit} \end{aligned} \tag{3.11}$$

where the numbers are given for $a = 0.25$. Note that these equations are valid for any $h$ and not only in the vicinity of $h_{\rm crit}$. One finds an exponent $x = 2.00(1)$ for $h < h_{\rm crit}$ and $h > h_{\rm crit}$. Extrapolated values for the $m_i$ are shown in figure 21.
The position of the minimum of the parabola equation (3.11) determines the spinodal point at $h_{\rm crit} = a/(1-a)$ with a precision of two digits.

- *upper gap:*
  The scale $m_2$ increases monotonically with $h$ over the entire range $0 \le h < 1$. One finds
  $$m_2 = 0.48(2) h^{1.22(2)} + 0.043(2) \tag{3.12}$$
  for $a = 0.25$.

- *lower band of excitations at $h = h_{\rm crit}$:*
  At the spinodal point, the lower band is of the following form:
  $$\begin{aligned} E_0 &= 0 \\ E_1 &= a\frac{k_1^{(1)}}{L} + \frac{\text{const.}}{L^{3/2}} + \cdots \quad \text{real} \\ E_j &= a\frac{k_j^{(1)}}{L} + \frac{\text{const.}}{L^{3/2}} + \cdots \quad j \ge 2,\ \text{complex conjugated pairs,} \end{aligned} \tag{3.13}$$
  with the extrapolated values $k_j^{(1)}$ given in table 3. One has universality: apart from the normalization constant $a$ ("speed of light"), the leading terms are the same for any critical point $h_{\rm crit}(a) = a/(1-a)$. Extrapolation of the $k_i^{(1)}$ for $a$ =0.25, 0.4, 0.1 gives the same result with 5 digits precision. At the spinodal phase transition, the dynamical critical exponent [32] is $z = 1$, as was found for the three-state diffusion model where,

however, this was only seen for the first excitation, see section 2.4.
The imaginary parts of the numbers $k_j^{(1)}$ follow (see table 3)

$$\mathrm{Im}(k_j^{(1)}) = 12.81(1)\, j \ . \tag{3.14}$$

This equidistant spacing comes as a surprise and we do not know its reason. For quantum spin chains related to a conformal field theory one expects regularities (conformal towers with certain degeneracies) for the real parts of the $k_j^{(1)}$. However, we could not detect any such structure looking at the real part of the spectrum. This should be a result of the reduced state space of the RWT model. Because of the large configuration space of the full three-state model, a similar analysis was not possible there.
For the higher band of excitations at the spinodal point, one again has the form of equation (3.10).

- *finite-size scaling analysis:*
  Finite-size scaling relations, which describe the behaviour of finite quantum spin chains in the vicinity of an (equilibrium) critical point of the infinite system [41], apply also to the (non-equilibrium) RWT model at $h_{\text{crit}}$. Consider the curves

  $$F_L:\ h \to L\, E_1(h,L) \ . \tag{3.15}$$

  The critical point $h_{\text{crit}}$ can be determined from extrapolation of the crossing points $h_{\text{cross}}(L)$ of the curves $F_L$ and $F_{L-1}$. Indeed one finds

  $$\lim_{L\to\infty} h_{\text{cross}}(L) = 0.3333(2) = h_{\text{crit}} \tag{3.16}$$

  for $a = 0.25$. This is the most precise numerical determination of $h_{\text{crit}}$.
  Following the finite-size scaling hypothesis, one can also determine the critical exponent $x$ in a way different from that of equation (3.11) [41]. From the available data up to $L = 220$, one again finds $x = 2.0(2)$.

In the following sections, we discuss further properties that can be related to the scales of the spectrum and to the universality at the critical point. The scale $\omega$ can be linked with flip times and the stationary FEF (see section 3.2). In section 3.4, we present dynamic quantities related to the properties of $H$, specifically to the gaps $m_i$.

### *3.2. The free energy functional and flip times between phases*

We have investigated the behaviour of the stationary probabilities $P_0(j,k)$ for different $h$. These probabilities were determined from the stationary state as computed by numerical diagonalization of the Hamiltonian (see the previous section). First, we remark that for $h = 0$ all eigenstates are also eigenstates of the $CP$ operation. We find that the eigenvectors corresponding to the complex conjugated pairs of eigenvalues $E_j^{(1)}$ of the lower band of excitations (3.9) are $CP^+$ for $j$ even and $CP^-$ for $j$ odd.

One also finds that, for any $h$ and finite $L$, the eigenvector $|P_0>$ with eigenvalue $E = 0$ is the only vector that directly corresponds to a probability distribution, i.e. all its entries are positive. In the case $h = 0$, $|P_0>$ has $CP^+$ symmetry.

Hence, for $h = 0$, the free energy functional $f(d)$, defined in equation (3.5), is symmetric under the inflection $d \to -d$. (From the data, one finds that the free energy functional is a well defined limit as was already known for the asymmetric exclusion model [22] and the three-state diffusion model above.) There are minima at $d = -1$ and $d = 1$ and a maximum at $d = 0$.

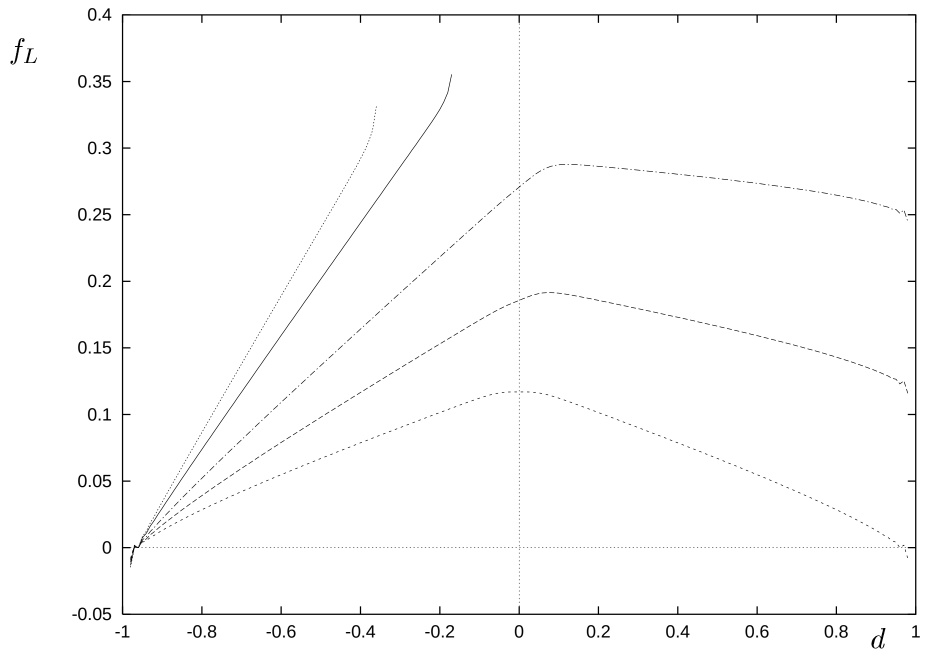


**Figure 22.** The free energy functional $f_L(d)$ for $a = 1/4$, $L = 100$ and $h = 0.0, 0.1, 0.2, 0.3333, 0.4$. The values are shifted by the value $f_L(-1)$. The data is generated by numerical diagonalization of the Hamiltonian. Since the precision is limited to $10^{-12}$ the curves for larger $h$ cannot be fully determined.

The minima correspond to the two equally stable phases (see figure 22). This is basically the same situation as for the $CP$-symmetric three-state model in the "low-temperature" phase.

For $0 < h < h_{\text{crit}}$, one finds a global minimum at $d = -1$ and a further, shallower minimum at $d = 1$ (see figure 22). This reflects the fact that one of the phases becomes meta-stable. One can define two scales:

$$\begin{aligned} \nu_{\text{large}} &= f_{\max} - f(-1) \\ \nu_{\text{small}} &= f_{\max} - f(1) \ , \end{aligned} \tag{3.17}$$

where $f_{\max}$ is the maximum value of $f(d)$. We shall relate these scales to the time the system needs to flip from one minimum to the other. At $h_{\text{crit}}$, the second minimum of $f$ (and hence the meta-stable phase) vanishes. This cannot be seen in figure 22 but can be inferred from the results for smaller lattice sizes. For $h \geq h_{\text{crit}}$, the free energy has only one minimum at $d = -1$.

Analysis of the eigenvectors of $H$ that become the steady states in the large $L$ limit, and the relation of the RWT to the three-state diffusion model, have given the result that below $h_{\text{crit}}$ there are two distinct phases with order parameter values $d = 1$ and $d = -1$. Above $h_{\text{crit}}$, however, there is only one phase: the walker stays near the favoured corner F of $T_L$. This can be verified with Monte Carlo simulations as above for the three-state diffusion model (see section 2.4). In a way similar to above one can measure the time for the RWT model to flip from one phase to the other. One finds that, for large $L$ and $h < h_{\text{crit}}$, in the neighbourhood of a corner F=$(1, L-1)$ or U=$(L-1, 1)$, the random walker moves through the configurations

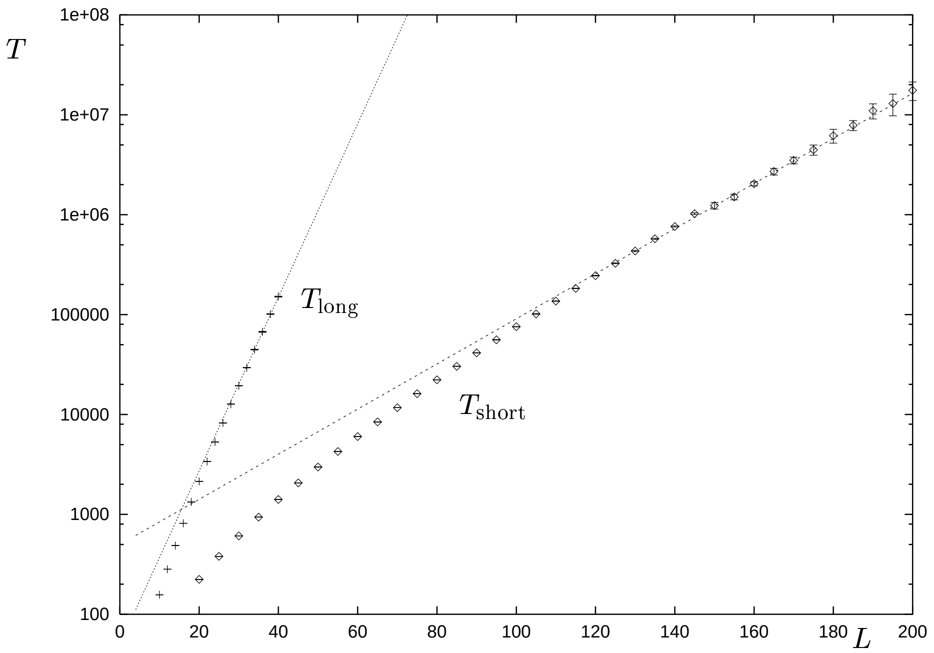


**Figure 23.** The flip times $T_{\rm short}(L)$ and $T_{\rm long}(L)$ for $a = 1/4$ and $h = 0.1$. The fitted lines are given by $50 \exp(0.2\, L)$ and $500 \exp(0.052\, L)$.

on a shorter time scale than is needed to get from one corner to the other. This allows one to measure the flip times $T_{\rm long}$ from favoured to unfavoured and $T_{\rm short}$ from unfavoured to favoured phase as average first passage times from F to U and U to F respectively.

With $c = 1/2$ and $a + b = 1/2$, the unit of time is defined such that, on average, the random walker moves one step (3.2) per unit. From the simulations, one finds that, in leading order, the flip times are given by

$$T_{\rm long} \propto \exp(\mu_{\rm long}\, L) \qquad \text{for any } h \tag{3.18}$$

$$T_{\rm short} \propto \begin{cases} \exp(\mu_{\rm short}\, L) & \text{for } h < h_{\rm crit} \\ L & \text{for } h \geq h_{\rm crit}\ . \end{cases} \tag{3.19}$$

For $h < h_{\rm crit}$, the time intervals the random walker spends alternately near either corner increase exponentially with $L$. The fraction of time in the meta-stable region decreases exponentially. In this sense, for $h < h_{\rm crit}$, there are a meta-stable and a stable phase. Results of the measurement for $a = 0.25$ and $h = 0.1$ are presented in figure 23.

For $h > h_{\rm crit}$, the proportionality constant in equation (3.19) can be calculated by a simple argument: In the interior of the triangle $T_L$, the random walker defined by (3.2) has an average velocity of

$$v = \begin{pmatrix} -h - a(1+h) \\ h - a(1-h) \end{pmatrix} \tag{3.20}$$

independent of the site $(j, k)$. Here, the first coordinate is along the $j$-axis (number of negative particles) and the second along the $k$-axis (positive particles). The projection onto the direction of the order parameter $d$ is given by

$$v_d = -2h(1-a) \tag{3.21}$$

Repeating the argument of [37], one sees that for small $h$ both components of $v$ are negative. The walker near either of the corners $(L-1,1)$ or $(1,L-1)$ drifts towards the $j$- or $k$-axis and subsequently jumps back to the respective corner. At $h_{\text{crit}} = a/(1-a)$, the velocity is antiparallel to the $j$-axis. For $h > h_{\text{crit}}$, the second component of $v$ is positive, rendering the unfavoured corner around $(L-1,1)$ unstable, because the random walker moves away from the $j$-axis and the non-local jumps along this axis become irrelevant in leading order. We have checked this with Monte Carlo simulations, (see also section 3.4).

Neglecting these non-local jumps, from the mean path given by $v$ one can easily calculate the time taken for a walker starting at $\text{U} = (L-1,1)$ to hit the $k$-axis and to reach the favoured corner. One finds the flip time

$$T_{\text{short}}^{h>h_{\text{crit}}} = \frac{L}{h+a(1-h)} = \frac{1+h_{\text{crit}}}{h+h_{\text{crit}}} L \, . \tag{3.22}$$

In contrast, the appearance of a linearly growing flip time at $h = h_{\text{crit}}$ is non-trivial. One finds the form

$$T_{\text{short}}^{h_{\text{crit}}} = \frac{L}{a} - \frac{\gamma L^{1/2}}{a} + \text{const.} \, , \tag{3.23}$$

where $\gamma = 0.57(6)$ is a positive constant and independent of $a$ to a precision of about 10%. Up to the normalization $a$, the short flip time is, in leading order, a universal function of $L$ as are the leading terms of the lower spectrum equation (3.13). The appearance of a universal linear flip time is linked to the universal $1/L$ spectrum of the Hamiltonian, compare equation (3.13). One can ask how general this universal behaviour is. Similar investigations for other models remain to be done.

Note that from (3.22) and (3.23) one finds that in leading order

$$\lim_{h\to h_{\text{crit}}} T_{\text{short}}^{h>h_{\text{crit}}} = 2T_{\text{short}}^{h_{\text{crit}}} \, . \tag{3.24}$$

Hence there is a discontinuity in the flip time $T_{\text{short}}^{h_{\text{crit}}}$. At the spinodal point, $T_{\text{short}}^{h_{\text{crit}}}$ has a special $L$ dependence, essentially different from its behaviour above or below this point.

The values of $\nu_{\text{small}}$ and $\nu_{\text{large}}$ in (3.17), determined from numerical diagonalization of $H$ for $L \leq 140$, and measurement of the flip times, up to $L = 200$ for $T_{\text{short}}$ and $L = 40$ for $T_{\text{long}}$, yield the following result:

$$\begin{aligned} \mu_{\text{short}} &= \nu_{\text{small}} && \text{for } h < h_{\text{crit}} \\ \mu_{\text{long}} &= \nu_{\text{large}} && \text{for any } h \, . \end{aligned} \tag{3.25}$$

As an example for $h = 0.1$ and $a = 0.25$, we find the values $\mu_{\text{short}} = 0.052(3)$ and $\mu_{\text{long}} = 0.20(2)$ (see figure 23) which is to be compared with $\nu_{\text{small}} = 0.053(2)$ and $\nu_{\text{large}} = 0.17(2)$ (see figure 22). For $h = 0$ and $a = 0.25$ the equations (3.25) can be checked to three digits; the precision decreases with increasing $h$ to about one digit at $h = 0.3$. (Finite-size corrections to (3.17), (3.18) and (3.19) become more important for higher $h$ due to crossover effects to the linear regime for $h \geq h_{\text{crit}}$.)

Equation (3.25) is interesting because it relates (steady state) properties of the free energy functional $f(d)$ with (dynamical) flips between phases. This is unexpected for a non-local model without detailed balance. For the further simplified RWRA model (see section 4) an analogous link can be made analytically. Also, for the three-state diffusion model, similar observations, albeit with less precision, were made in section 2.4.

One also finds that $\mu_{\rm short} = \omega$ (recall that $E_1 \propto \exp(-\omega L)$ is the first excitation of the Hamiltonian, see equation (3.8)). For $h = 0.1$ and $a = 0.25$ the value of $\omega$ from numerical diagonalization is 0.048(3). The reason for this connection, together with an analogous expression for $\mu_{\rm long}$, is given in next section, where we consider modified models with absorbing configurations.

### *3.3. The RWT model with absorbing configurations*

In this section, we investigate further the relation of flip times and spectra. We focus on the case where the time that the walker remains in a phase increases exponentially with the system size.

The flip times $T_{\rm long}$ (3.18) and $T_{\rm short}$ (3.19) are defined as first passage times. It is known that the corresponding time scales are related to dynamical properties, i.e. excitations, of a modified model with an absorbing state [42, 43]. An absorbing state is a configuration the system cannot escape from. Here we have to choose U (for $T_{\rm long}$) or F (for $T_{\rm short}$) as the absorbing configuration.

We shall first present the general argument (see [42, 43]). Consider a reaction diffusion system with an absorbing configuration $\{\beta_{\rm abs}\}$ and described by a master equation (3.4) with a Hamiltonian $H_{\rm abs}$. The system may start in a configuration $\{\beta_0\}$ at time $t = 0$:

$$|P(t=0)>_{\{\beta\}} = \begin{cases} 1 \text{ for } \{\beta\} = \{\beta_0\} \\ 0 \text{ for } \{\beta\} \neq \{\beta_0\} \end{cases} \tag{3.26}$$

where the subscript of a vector denotes the component $\{\beta\}$. Let $E_\lambda$ and $|P_\lambda>$ be eigenvalues and eigenvectors of the Hamiltonian ($E_0 = 0$ being the ground state energy). Note that the ground state $|P_0>$ is given by

$$|P_0>_{\{\beta\}} = \begin{cases} 1 \text{ for } \{\beta\} = \{\beta_{\rm abs}\} \\ 0 \text{ for } \{\beta\} \neq \{\beta_{\rm abs}\} \end{cases} \tag{3.27}$$

If $H_{\rm abs}$ is diagonalizable, there exist $a_\lambda \in \mathbb{C}$ such that

$$|P(t=0)> = \sum_\lambda a_\lambda \, |P_\lambda> \quad . \tag{3.28}$$

Obviously, the probability $P_{\rm in}$ that the system has not reached its absorbing state is given by

$$\begin{aligned} P_{\rm in}(t) &= 1 - P(\{\beta_{\rm abs}\};t) \\ &= 1 - (\exp(-H_{\rm abs}\, t)\, |P(t=0)>)_{\{\beta_{\rm abs}\}} \\ &= 1 - \sum_\lambda a_\lambda \exp(-E_\lambda\, t)\, |P_\lambda>_{\{\beta_{\rm abs}\}} \quad . \end{aligned} \tag{3.29}$$

Denote as $p(t){\rm d}t$ the probability that the system reaches $\{\beta_{\rm abs}\}$ during the time interval $[t, t+{\rm d}t]$. Then

$$p(t){\rm d}t = P_{\rm in}(t) - P_{\rm in}(t+{\rm d}t) \quad . \tag{3.30}$$

Thus, $p(t)$ is given by

$$p(t) = -\frac{\mathrm{d}P_{\mathrm{in}}(t)}{\mathrm{d}t} = -\sum_{\lambda} a_\lambda E_\lambda \exp(-E_\lambda t) \, |P_\lambda >_{\{\beta_{\mathrm{abs}}\}} , \tag{3.31}$$

and its mean value, the flip time, is

$$T = -\sum_{\lambda \neq 0} \frac{a_\lambda \, |P_\lambda >_{\{\beta_{\mathrm{abs}}\}}}{E_\lambda} . \tag{3.32}$$

From the last equation, it follows, under the conditions

$$E_1 \propto \exp(-m\,L) , \qquad \lim_{L\to\infty} E_i > 0 \text{ for } i \neq 0, 1 , \qquad \exists y > 0 : \lim_{L\to\infty} L^y a_1 \neq 0 ,$$

that in leading order

$$T(L) \propto \exp(m\,L) . \tag{3.33}$$

The result is similar for any finite number of excited states $E_i \propto \exp(-m_i\,L)$. In that case, the scale of the flip time is given by the largest $m_i$, with $\lim_{L\to\infty} L^y a_i \neq 0$ for some $y$.

On the other hand, if none of the excited levels approaches zero for $L \to \infty$, one has

$$T(L) \leq \mathcal{O}\left(\dim(L)\right) \tag{3.34}$$

independent of $\{\beta_0\}$ ($\dim(L)$ is the dimension of the configuration space for system size $L$). This implies that there is only one phase in the large $L$ limit.

We now turn to specific results for the RWT model. We have diagonalized the modified Hamiltonian numerically. From the spectra we find the length scales $\mu_{\mathrm{long}}$ and $\mu_{\mathrm{short}}$ of the flip times:

- With the favoured corner F made absorbing, the scale $\omega$ (3.8) remains unchanged as does the gap of the lower band of excitations $m_1$. This explains the relation $\mu_{\mathrm{short}} = \omega$ (3.25) which is a special case of (3.33). Similar relations are found analytically for the further simplified RWRA model discussed in chapter 4.
  The lower gap vanishes at the critical point $h_{\mathrm{crit}}$ and the $1/L$ dependence of the levels is the same as for the non-absorbing RWT model (table 3). The upper gap changes to a new value $m_3 > m_2$.
  These results confirm the interpretation that the second ground state (which exists for $h < h_{\mathrm{crit}}$, $L \to \infty$) and the lower band of excitations are linked with the metastable phase and with the movement from the unfavoured to the favoured corner. The corresponding scales of the spectrum remain unchanged, while the movement within the favoured phase, and correspondingly the upper band of excitations, is altered by the absorbing configuration F.

- In the case of an absorbing configuration U in the (originally) unfavoured phase, there is more change to the spectrum. There is a first excited state $E_1 \propto \exp(-\omega'\,L)$ with $\omega' \neq \omega$ for any $h$, connected with two steady states for $L \to \infty$. This reflects the fact that, with absorption in the corner U, both corners U and F constitute a phase for any $h$. From (3.33) one has

$$\mu_{\mathrm{long}} = \omega' \quad \text{for any } h, \tag{3.35}$$

analogous to (3.25). This relation is consistent with the numerical data to a precision of about 15%.
Further, the scale $\omega'$ is related to $m_2$ of the RWT model without an absorbing configuration. For $a = 0.25$ one has

$$\omega' = 2.5(2)\, m_2 \quad . \tag{3.36}$$

As a further change to the spectrum, the lower band of excitations is shifted to a new band of excitations with a gap $m_3 > m_2$, while the gap $m_2$ remains unchanged.
The new upper band of excitations is related to movement within the former unfavoured corner. Note that $m_3(h)$ takes the same values with either the favoured or the unfavoured corner made absorbing. The corresponding eigenstates describe the (rapid) movement near an absorbing corner.

*3.4. Time scales and criticality in the movement of the random walker*

To find macroscopic physical quantities reflecting the time scales of the spectrum and the critical behaviour at $h_{\rm crit}$, we investigated the movement of the random walker starting from the specific initial positions U$= (L-1, 1)$ (the unfavoured corner) or F$= (L-1, 1)$ (the favoured corner). In the following we concentrate on the time dependence of the order parameter coordinate. Defining the average order parameter distance from the starting point as

$$s(t) = \frac{|< d(t) - d(0) >|}{2} \, , \tag{3.37}$$

the start configuration corresponds to $s = 0$ and the opposite corner of the triangle $T_L$ to $s = 1$.

*Start at unfavoured corner*

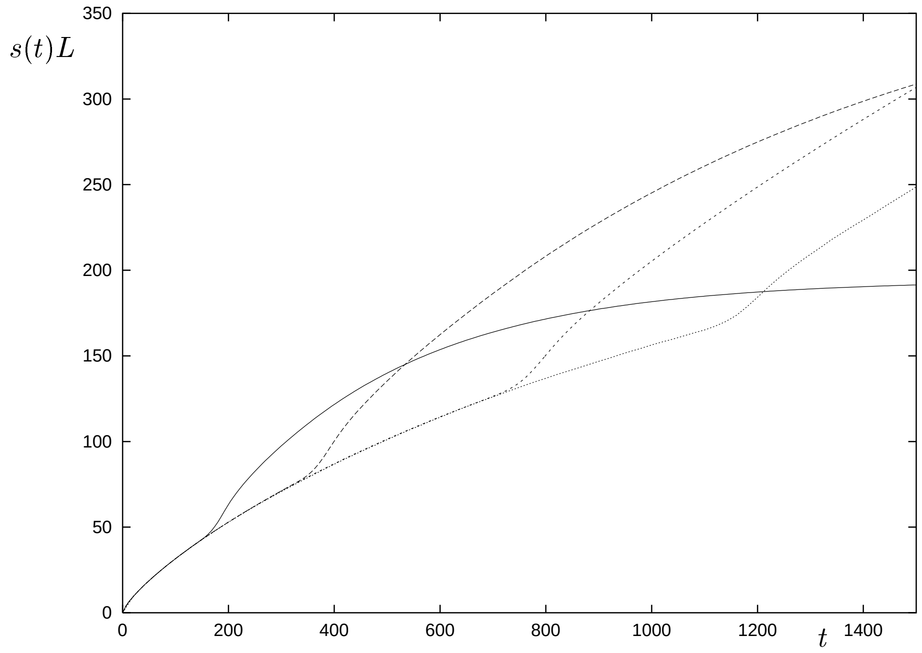


**Figure 24.** Average distance $s(t)$ from starting point U=$(L-1, 1)$.
Data from simulation of the RWT model for $a = 1/4$, $h = 0.3$ and system sizes $L = 100, 200, 400, 600$. The scaling variable is $t$.

First, we consider the random walker starting at the point U. We shall see that the movement from the unfavoured to the favoured corner is linked with the lower excitations of the Hamiltonian.

Typical pictures of the walker position $s(t)$ are given in figures 24, 25, 26 and 27. In figure 24 we show the product $L \cdot s$ as a scaling function of $t$, in figure 25 the distance $s$ as a scaling function of $t/T_{\rm short}$ (both for $h$ below the critical point), and in figures 26 and 27 the distance $s$ as a scaling function of $t/L$ (at and above the critical point respectively). One observes the following properties of the scaling functions:

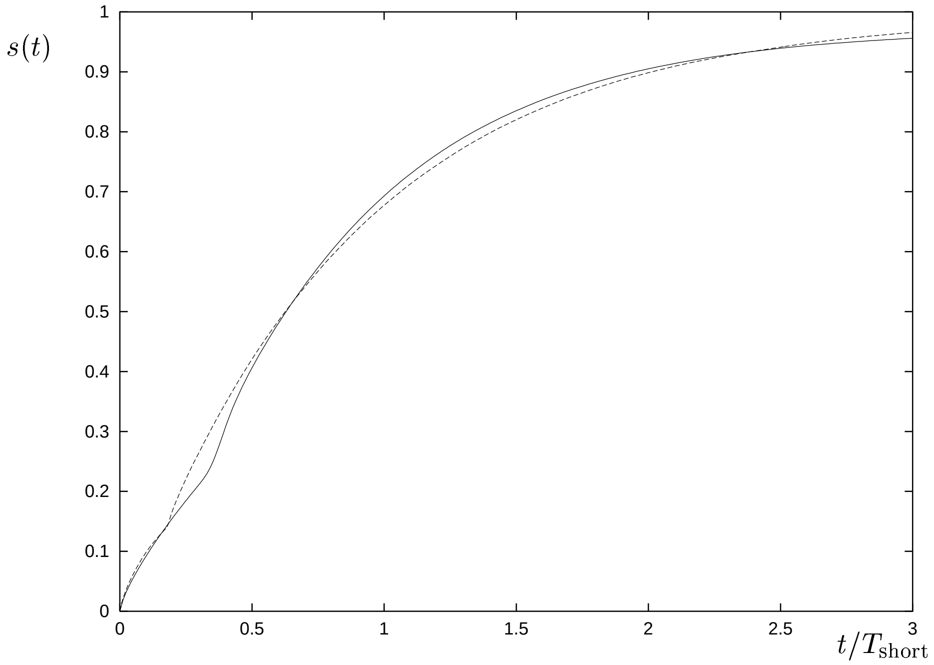


**Figure 25.** Average distance $s(t)$ from starting point U=$(L-1,1)$. Data from simulation of the RWT model for $a = 1/4$, $h = 0.3 < h_{\text{crit}}$. The solid curve represents the data for $L = 100$, the dashed for $L = 600$.

- $h < h_{\text{crit}}$:
  The random walker stays near U for an average time exponentially increasing with $L$ (see equation (3.19)). For large $L$, the path near the unfavoured corner (start) is described by the scaling function
  $$Ls(t) \propto (1 - \exp(-\lambda t)) \ . \tag{3.38}$$
  Here we find $\lambda = 1.8(2) \cdot m_1(h)$ for $a = 0.25$. Due to the distribution of flip times for finite $L$, the walker leaves this regime at different times (figure 24).
  For the approach to the favoured corner, one observes a different scaling (figure 25). From the data, one finds that $s$ is given by
  $$s(t, L) = s_\infty - \exp(-\lambda \frac{t}{T_{\text{short}}(L)}) \ , \tag{3.39}$$
  where
  $$s_\infty = \lim_{t\to\infty} s(t) = 1 - \frac{\text{const.}}{L} + \cdots \ . \tag{3.40}$$
  In equation (3.39), the constant $\lambda = 1.15(3)$ is independent of $a$. The approach to the favoured corner scales with $t/T_{\text{short}}$. In the scaling of figure 25, the initial path (see equation (3.38) and figure 24) of the random walker cannot be seen because it is reduced to a point.

- $h = h_{\text{crit}}$:
  We consider the scaling regime $t \to \infty$ and $L \to \infty$, taking $t/L$ fixed. For $t < T_{\text{short}}/2 = L/2a$, the distance from the starting point increases in leading order linearly with time.

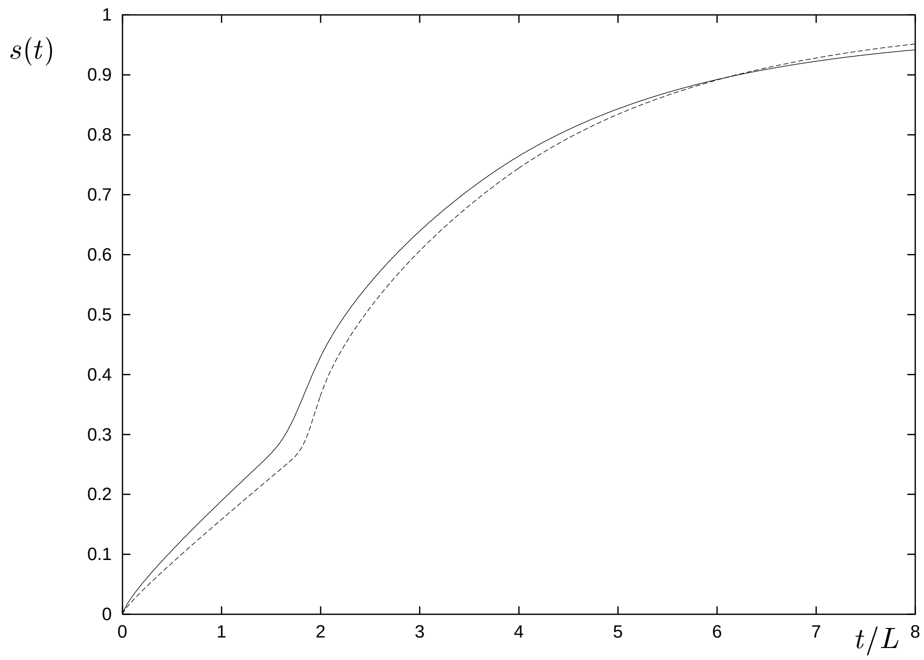


**Figure 26.** Average distance $s(t)$ from starting point U=$(L-1,1)$.
Data from simulation of the RWT model for $a = 1/4$, $h = h_{\mathrm{crit}}$. The solid curve represents the data for $L = 100$, the dashed for $L = 400$.

We find

$$s(t, L) = \frac{1}{L}\left(\frac{a}{2}t + \delta\sqrt{t} + \text{const.} + \cdots\right) , \tag{3.41}$$

where $\delta = 0.17(2)$ independent of $a$.
For large $t > T_{\mathrm{short}}/2$, the random walker approaches $s = 1$ exponentially, as in the case $h \neq h_{\mathrm{crit}}$. The scale, however, is the size of the system

$$s(t, L) = s_\infty - (s_\infty - a)\exp(-\kappa(a\frac{t}{L} - \frac{1}{2})) , \tag{3.42}$$

with $\kappa = 1.7(1)$ independent of $a$. Typical data is shown in figure 26.
At the critical point, the initial path of the random walker equation (3.41) is universal and linear in leading order. This reflects again the universal $1/L$ spectrum found for the critical point (3.13). It is remarkable that the exponential scale of equation (3.42) is also universal (but not the scaling function). Up to the time normalization (as in section 3.1), they do not depend on $a$ and scale with $tL^{-1}$.

- $h > h_{\mathrm{crit}}$:
  Again we study the scaling $t/L$ fixed taking $t$ and $L$ to infinity. Starting from the unfavoured corner U, at first (for $t < T_{\mathrm{short}}$) and in leading order the random walker follows a mean path determined by its velocity vector (3.20). The corrections are exponential in $t$. We find

$$s(t, L) = ah\frac{t}{L} - \frac{\zeta(1 - \exp(\xi t))}{2L} . \tag{3.43}$$

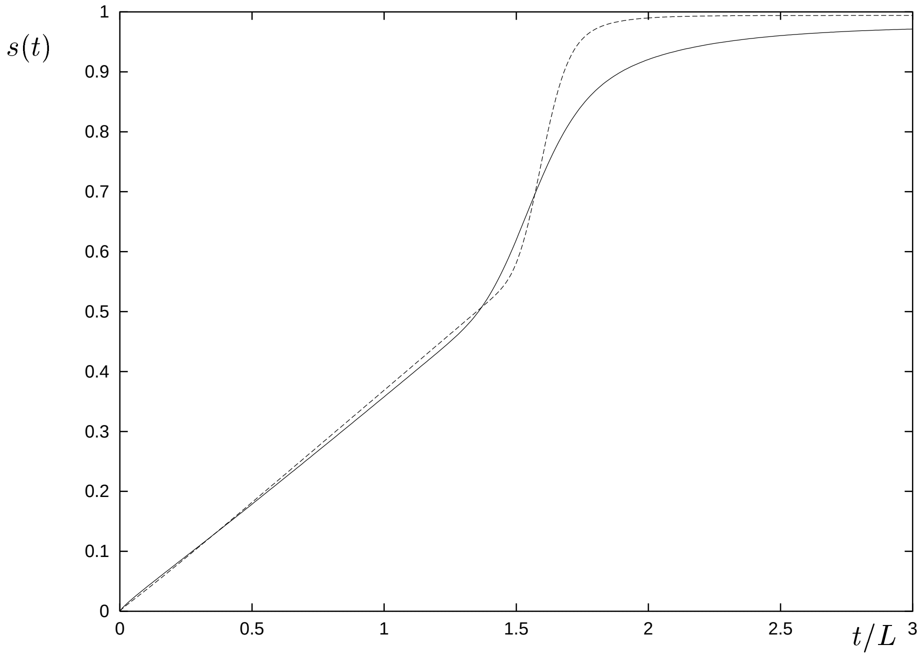


**Figure 27.** Average distance $s(t)$ from starting point U=$(L-1,1)$.
Data from simulation of the RWT model for $a = 1/4$, $h = 1/2 > h_{\text{crit}}$. The solid curve represents the data for $L = 100$, the dashed for $L = 400$. The scaling variable is $t/L$.

With increasing $h$, the constant $\zeta$ decreases and $\xi$ increases and thus the corrections become smaller, consistent with the explanation in section 3.2.
For $t > T_{\text{short}}$, one again finds an exponential approach to the final value $s = 1$ (see figure 27). One has

$$s(t, L) = s_\infty - \eta \exp(-(m_1 + \frac{\chi}{L})(t - T_{\text{short}}))\,, \tag{3.44}$$

where $T_{\text{short}}$ is given by (3.22). The scale is the gap $m_1$ from the spectrum of the time evolution operator. Following section 3.2, one finds the prefactor from equation (3.21)

$$\eta = \frac{1}{1 + h/h_{\text{crit}}}\,. \tag{3.45}$$

*Start at the favoured corner*

We have also studied the path of the random walker starting from F. In that case the critical point $h_{\text{crit}}$ does not play a special role. From the simulations, one finds

$$s(t, L) \propto \frac{1 - \exp(\lambda t)}{L}\,, \tag{3.46}$$

where $\lambda = 1.25(5) \cdot m_2(h)$ for $a = 0.25$. This equation is similar to equation (3.38), but note that in this case the movement is related to the time scale $m_2$ that describes a faster movement than the time scale $m_1$.

In summary, from the study of the movement of the random walker described in this section one can identify different scales. They are related to those excitations of $H$ that describe the movement in question. One finds that the lower band of excitations (slow modes) is related to the path from F to U and the higher band (fast modes) to the movement around the favoured corner F. This is confirmed by the results of section 3.3 for the model with absorbing configurations. For $h_{\mathrm{crit}}$, we find a scaling function involving only the system size $L$ as a scale, and depending on $tL^{-1}$. This scaling is analogous to the case of conformal invariance in critical equilibrium systems.

We want to point out that, of course, the described scaling properties can also be found by investigating order parameters different from $d$.

## 4. The RWRA model

The random walker on a triangle can be further simplified to a random walker on a right angle (RWRA) model which can be handled analytically while still possessing a meta-stable phase. This is done taking $b = 0$ and keeping only the points $(j, k) \in T_L$ with $j = 1$ or $k = 1$. That is, we consider only the movement along the $j$- and $k$-axes, where macroscopic jumps occur. In an infinitesimal time interval $\mathrm{d}t$ the following processes can occur with a probability $p$:

$$\begin{aligned}
&(j,1) \to (j-1,1) && \text{if } j > 1 \text{ with } p = a(1+h)\mathrm{d}t \\
&(j,1) \to (L-1,1) && \text{with } p = c(1-h)\mathrm{d}t \\
&(1,k) \to (1,k-1) && \text{if } k > 1 \text{ with } p = a(1-h)\mathrm{d}t \\
&(1,k) \to (1,L-1) && \text{with } p = c(1+h)\mathrm{d}t
\end{aligned} \tag{4.1}$$

The RWRA model is essentially an one-dimensional (albeit non-local) random walker model. Again we limit our investigation to the case $c = 1/2$ (this fixes the unit of time) and $a \equiv a + b = 1/2$. We checked that taking $a$ different from $1/2$ does not change the physics of the RWRA model. One is able to calculate exactly a characteristic equation for the eigenvalues of the time evolution operator, the free energy functional and the flip times. The spinodal point is at $h_{\text{crit}} = a/(1-a) = 1$. Since all rates in (4.1) have to be positive one can study with the RWRA model only the regime below the spinodal point.

We shall indeed see that for the RWRA model there are first passage times from one corner to the other which increase exponentially with $L$ as for the RWT model. We calculate their exact expressions in section 4.1 and find the two scales with which these flip times diverge.

We are also able to compute the first excitation, which becomes a second ground state in the large $L$ limit, and the first excitation for the RWRA model with either of the corners made absorbing. The first excitations are proportional to $\exp(-\omega L)$. In the case of no absorption or absorption at the favoured corner, $\omega$ is equal to the scale of the short flip time; and, in the case of the unfavoured corner made absorbing, $\omega$ is equal to the scale of the long flip time. All these results are analogous to those for the RWT model, but here they are obtained analytically (see section 4.2).

In section 4.3, the free energy functional is computed. It shows the same behaviour as that for the RWT model. As above, the height differences $f_{\text{max}} - f_{\text{min}}$ give the scales with which the flip times diverge.

### *4.1. The flip times*

As for the RWT model, for $h = 0$ the random walker stays most of the time near the points F=$(1, L-1)$ and U=$(L-1, 1)$. For $h > 0$, the point F is favoured and the stable phase is concentrated around this site.

To calculate the flip time from the meta-stable to the stable phase, we define $D_{j,k}$ as the first passage time from $(j, k)$ to $(1, L-1)$.

Concentrating on the first step of the random walker (in an infinitesimal time interval $\mathrm{d}t$), we find

$$\begin{aligned}
D_{1,k} = {} & (1-\mathrm{d}t)(D_{1,k} + \mathrm{d}t) \\
& + \frac{1-h}{2}\mathrm{d}t(D_{1,k-1} + \mathrm{d}t)
\end{aligned}$$

$$+\frac{1+h}{2}\mathrm{d}t(D_{1,L-1}+\mathrm{d}t).$$

for $j=1,k=2,\ldots,L-2$ (cf. [37]). This yields

$$D_{1,k}=1+\frac{1-h}{2}D_{1,k-1}+\frac{1+h}{2}D_{1,L-1}. \tag{4.2}$$

Similarly, the other conditions for the $D_{j,k}$ read

$$D_{j,1}=1+\frac{1+h}{2}D_{j-1,1}+\frac{1-h}{2}D_{L-1,1} \qquad j=2,\ldots,L-2 \tag{4.3}$$

$$D_{1,1}=1+\frac{1+h}{2}D_{1,L-1}+\frac{1-h}{2}D_{L-1,1} \tag{4.4}$$

$$\frac{1-h}{2}D_{1,L-1}=1+\frac{1-h}{2}D_{1,L-2} \tag{4.5}$$

$$\frac{1+h}{2}D_{L-1,1}=1+\frac{1+h}{2}D_{L-2,1}\ . \tag{4.6}$$

From the definition of $D_{j,k}$, the boundary conditions are given by

$$\begin{aligned}&D_{1,L-1}=0\\&D_{L-1,1}=T_{\text{short}}\ .\end{aligned} \tag{4.7}$$

The recurrence relation (4.3) can be solved as

$$D_{j,1}=D_{1,1}\frac{2}{1-h}\left(\left(\frac{1+h}{2}\right)^{j-2}-\left(\frac{1+h}{2}\right)^{j}+1\right)\ , \tag{4.8}$$

and the condition (4.6) gives us the flip time

$$T_{\text{short}}=\left(\frac{2}{1-h}\right)^2\left(\frac{2}{1+h}\right)^{L-2}-\frac{2}{1-h}\ . \tag{4.9}$$

Replacing $h$ by $-h$, we obtain the flip time from favoured to unfavoured phase

$$T_{\text{long}}=\left(\frac{2}{1+h}\right)^2\left(\frac{2}{1-h}\right)^{L-2}-\frac{2}{1+h}. \tag{4.10}$$

One sees that the flip times diverge exponentially with $L$. The scales are $\mu_{\text{short}}=\log(2/(1-h))$ and $\mu_{\text{long}}=\log(2/(1+h))$. This implies that there are two ground states in the large $L$ limit. Linear combinations of these give the phases; a stable phase concentrated around F$=(1,L-1)$, and a meta-stable around U$=(L-1,1)$.

### *4.2. The finite-size corrections to the first excitation*

With the notation $x_s=P(s,1)$, $y_s=P(1,s)$ and $x_1=y_1=P(1,1)$, the master equation of the RWRA model reads

$$\frac{\mathrm{d}}{\mathrm{d}t}x_s=-x_s+\frac{1+h}{2}x_{s+1} \qquad s=2,\ldots,L-2 \tag{4.11}$$

$$\frac{\mathrm{d}}{\mathrm{d}t}y_s=-y_s+\frac{1-h}{2}y_{s+1} \qquad s=2,\ldots,L-2 \tag{4.12}$$

$$\frac{\mathrm{d}}{\mathrm{d}t}x_1=-x_1+\frac{1+h}{2}x_2+\frac{1-h}{2}y_2 \tag{4.13}$$

$$\frac{\mathrm{d}}{\mathrm{d}t}x_{L-1} = -x_{L-1} + \frac{1-h}{2}\sum_{i=1}^{L-1} x_i \tag{4.14}$$

$$\frac{\mathrm{d}}{\mathrm{d}t}y_{L-1} = -y_{L-1} + \frac{1+h}{2}\sum_{i=1}^{L-1} y_i \; . \tag{4.15}$$

Setting $x_s = \exp(-Et)X_s$ and $y_s = \exp(-Et)Y_s$, and solving the resulting recurrence relations, we find the condition on an eigenvalue $E$,

$$\begin{aligned} 0 = E\Bigg( & E(1-E)^{2L-3} + \frac{(1-h^2)^{L-1}}{4^{L-1}} \\ & - (1-E)^{L-2}(1-h^2)\frac{(1+h)^{L-2}+(1-h)^{L-2}}{2^L}\Bigg) \\ & \left((1-E)^{2L-5}(\frac{1+h}{2}-E)(\frac{1-h}{2}-E)\right)^{-1} . \end{aligned} \tag{4.16}$$

There is one solution with $E_0 = 0$. The corresponding eigenvector is the steady state for finite $L$. For $L \gg 1$, the first excited level behaves as

$$E_1 \cong \frac{1}{4}(1-h^2)\left(\frac{1+h}{2}\right)^{L-2} \propto \exp(\omega L) \; . \tag{4.17}$$

Thus, for $L \to \infty$, one has two stationary states resulting in two phases.

The higher spectrum has a two band structure similar to that for the RWT model. The corresponding gaps are $m_1 = (1-h)/2$ and $m_2 = (1+h)/2$. Thus, one finds $\omega = m_1$ for $h \to 1$. (For the RWT model one has proportionality of $\omega$ and $m_1$ for any $h$, see (3.11).) We point out that for the RWRA model the gap vanishes with a critical exponent $x = 1$, while for the RWT model one finds $x = 2$ (see equation (3.11)). This is due to the reduction of the configuration space.

One can compute the large $L$ behaviour of the flip times from the $L$-dependence of the first excited level of a modified model with an absorbing configuration as in section 3.3. For the flip time $T_{\text{short}}$, one implements an absorbing site at the stable corner $(1, L-1)$, replacing equations (4.12) and (4.15) by

$$\frac{\mathrm{d}}{\mathrm{d}t}y_s = -y_s + \frac{1-h}{2}y_{s+1} \qquad s = 2,\ldots,L-3 \tag{4.18}$$

$$\frac{\mathrm{d}}{\mathrm{d}t}y_{L-2} = -y_{L-2} \tag{4.19}$$

$$\frac{\mathrm{d}}{\mathrm{d}t}y_{L-1} = \frac{1+h}{2}\sum_{i+1}^{L-2} y_i \; . \tag{4.20}$$

With this, one finds a first excited level

$$E_1^{(1,L-1)\text{abs.}} \cong \frac{1}{4}(1-h^2)\left(\frac{1+h}{2}\right)^{L-2} . \tag{4.21}$$

With $(L-1, 1)$ absorbing, instead of $(1, L-1)$, one analogously obtains

$$E_1^{(L-1,1)\text{abs.}} \cong \frac{1}{4}(1-h^2)\left(\frac{1-h}{2}\right)^{L-2} . \tag{4.22}$$

This way, with equations (4.9),(4.10) and (3.33), we find

$$\begin{aligned} T_{\text{short}} &\propto \left(\frac{2}{1+h}\right)^{L-2} \\ T_{\text{long}} &\propto \left(\frac{2}{1-h}\right)^{L-2} \quad , \end{aligned}$$

which is indeed consistent with the flip times (4.9) and (4.10) computed directly above.

### *4.3. The stationary probability distribution*

To calculate the probability distribution of the steady state, one has to solve equations (4.11)–(4.15) for $(\mathrm{d}/\mathrm{d}t)\, x_s = (\mathrm{d}/\mathrm{d}t)\, y_s = 0$. One finds

$$X_s = \frac{1}{4} N(1-h^2) \left(\frac{2}{1+h}\right)^{s} \tag{4.23}$$

$$Y_s = \frac{1}{4} N(1-h^2) \left(\frac{2}{1-h}\right)^{s} \qquad s = 2, \ldots, L-1 \tag{4.24}$$

$$X_1 = Y_1 = N \ , \tag{4.25}$$

where the normalization $N$ is

$$N = \frac{(1-h^2)^{L-2}}{(2(1-h))^{L-2} + (2(1+h))^{L-2} - (1-h^2)^{L-2}} \ . \tag{4.26}$$

The free energy, defined by (3.5), takes the form

$$f(d) = \begin{cases} \log\left(2/(1-h)\right) - d \log\left(2/(1+h)\right) & \text{for } d \geq 0 \\ \log\left(2/(1-h)\right) + d \log\left(2/(1-h)\right) & \text{for } d \leq 0 \ . \end{cases} \tag{4.27}$$

The minima of the free energy functional are at $d = -1$ and $d = 1$, corresponding to the stable and meta-stable phase respectively. In between, the free energy functional has a constant slope.

In conclusion, we have shown that the RWRA model presented in this section captures most of the physics of the RWT model below the critical point.

## 5. Conclusion

We have studied spontaneous $CP$ symmetry breaking and spinodal points of stationary states in the framework of a three-state diffusion model.

In the disordered high-temperature (the parameter $\beta$ plays the role of a temperature) phase the free energy functional as a function of the order parameter has only one minimum. We have a first-order phase transition at $\beta_{\text{crit}}$ with a flat free energy functional (like in equilibrium problems). At $\beta_{\text{crit}}$ the density profiles and correlation functions in the scaling regime can be explained using a certain combination of shocks. Below the critical temperature $\beta_{\text{crit}}$, in the broken phase, the free energy functional is not a convex function of the order parameter (unlike in equilibrium problems) but has two minima corresponding to two phases defined by their average densities of positive and negative particles. If the $CP$ symmetry of the model is broken by a small perturbation (parameter $h$), one has only one minimum for the first-order phase transition (like in equilibrium) but still two minima in the broken phase. If we increase $h$ one gets spinodal points. We have seen that the free energy functional behaves like in Ginzburg-Landau theory.

At the first-order phase transition we have seen massless excitations in the spectrum of the quantum chain Hamiltonian associated with the dynamics of the process with a critical dynamical exponent $z = 2$. This does not exclude the presence of massive excitations which are suggested by the exponential tails seen in the density profiles.

At the spinodal points we have also seen massless excitations with $z = 1$. These observations are confirmed by the investigation of the $\beta \to 0$ limit of the three-state diffusion model, the RWT model. The reduced size of the configuration space of this single particle model allows us to determine the spectrum numerically with sufficient precision to extract two gaps (time scales) and the large $L$ limit of the low excitations. For many-particle models, as the three-state diffusion model, a numerical investigation of the spectrum is much more difficult.

At the spinodal point, $h_{\text{crit}}$, in the RWT model, one of the gaps in the spectrum vanishes and for the corresponding excitations we find $E_i = a\, k_i/L$, i.e. the dynamical exponent is $z = 1$, and these excitations are universal in the sense that the constants $k_i$ do not depend on the remaining parameters of the model. We believe that the $1/L$ dependence on the system size is a more general phenomenon and expect more structure to be found for the spectrum of many-particle models at their spinodal points. Besides that we found an integer spacing in the imaginary parts of the constants $k_i$. The missing conformal towers for the RWT model may be a result of the reduced configuration space. Whether such a spectrum has further deep implications, as would be the case for equilibrium problems where one has conformal invariance, remains uncertain.

As for the three-state model, we have also investigated the free energy functional as a function of the order parameter. Surprisingly for a non-local model without detailed balance (but analogous to the three-state model), we observed a link between steady state properties (the free energy functional) and non-stationary dynamics (flip times).

Those of the described results that are related to the region $h < h_{\text{crit}}$ can also be found in a simplified, one-dimensional random walker model, the RWRA model. For this model one can calculate the free energy functional, first excitations and flip times analytically.

Let us come back to our initial motivation to study non-equilibrium models. We have seen, that some concepts of equilibrium statistical mechanics, as the free energy functional, can be of much help in the investigation of non-equilibrium phenomena. It has to be defined in a different way, since a Gibbs-Hamiltonian as in equilibrium models is not at ones hand in non-equilibrium models. Further, it does not have to convex for these models. Instead it may have several minima, corresponding to stable and meta-stable phases. This is due to the fact, that non-equilibrium stationary states are a wider class of distributions than equilibrium states. The former are able to show much more interesting physics than the latter.

Recent investigations of a three-state model on a ring show spontaneous breaking of translational symmetry in one dimension. Further, the definition of a "grand canonical ensemble" enables to describe the observed phenomena in this model in the framework of Bose-Einstein condensation [44, 45]. Which other concepts of equilibrium statistical mechanics can be applied to non-equilibrium behaviour has to be investigated.

**Acknowledgment**

I want to thank Thomas Heinzel and Vladimir Rittenberg. The former as a friend for very fruitful collaboration, the latter for introducing me into the subject and teaching me to ask the right questions.

I want to thank the theory group in Bonn, the high-energy group in Trieste and my friends who gave me the right surrounding to "survive".

## References


[1] J. W. Gibbs 1902, *The elementary Principles in Statistical Mechanics* (Scribner, N.Y.)

[2] F. C. Alcaraz, M. Droz, M. Henkel, V.Rittenberg 1994, *Ann. Phys. (N.Y.)* **230** 250

[3] V. Privman (ed.) 1997, *Nonequilibrium statistical Mechanics in one dimension* (Cambridge University Press, Cambridge)

[4] B. Derrida, M. R. Evans, V. Hakim and V. Pasquier 1992, *J. Stat. Phys.* **69** 667

[5] B. Derrida, M. R. Evans, V. Hakim and V. Pasquier 1993, *J. Phys. A: Math. Gen.* **26** 1493

[6] G. Schütz and E. Domany 1993, *J. Stat. Phys.* **72** 277

[7] B. Derrida, S. A. Janowsky, J.L. Lebowitz and E. R. Speer 1993 *Europhys. Lett.* **22** 651

[8] B. Derrida, S. A. Janowsky, J.L. Lebowitz and E. R. Speer 1993 *J. Stat. Phys.* **73** 813

[9] F. H. L. Eßler and V. Rittenberg 1996, *J. Phys. A: Math. Gen.* **29** 3375

[10] F. C. Alcaraz, S. Dasmahapatra and V. Rittenberg 1998, *J. Phys. A: Math. Gen.* **31** 845

[11] P. F. Arndt, T. Heinzel and V. Rittenberg 1998, *J. Phys. A: Math. Gen.* **31** 833

[12] B. Derrida, M. R. Evans and K. Mallick 1995, *J. Stat. Phys.* **79** 833

[13] K. Mallick 1996, *J. Phys. A: Math. Gen.* **29** 5375

[14] S. A. Janowsky and J. L. Lebowitz 1992, *Phys. Rev.* **A45** 618

[15] G. Schütz 1993, *J. Stat. Phys.* **71** 471

[16] K. Krebs and S. Sandow 1997, *J. Phys. A: Math. Gen.* **30** 3165

[17] B. Schmittmann and R. K. P. Zia 1995 in: *Phase Transitions and Critical Phenomena* Vol. 17 eds. C. Domb and J. L. Lebowitz (Academic Press, N.Y.)

[18] G. Korniss, B. Schmittmann and R. K. P. Zia 1997, *J. Stat. Phys.* **86** 721

[19] S. Puri, A. J. Bray and J. L. Lebowitz 1997, *Phase separation kinetics in a model with order-parameter dependent mobility*, `cond-mat 9709113`, to appear in *Phys. Rev. E*

[20] G. Parisi 1988 *Statistical Field Theory* (Reading, MA)

[21] J. M. J. van Leeuwen and H. J. Hilhorst 1981 *Physica* A**107** 319;
G. Forgacs, R. Lipowsky and Th. M. Nienwenhuizen 1991 in: *Phase Transitions and Critical Phenomena* Vol. 14 eds. C. Domb and J. L. Lebowitz (Academic Press, N.Y.)

[22] P. F. Arndt, T. Heinzel and V. Rittenberg 1998, *J. Stat. Phys.* **90** 783

[23] P. F. Arndt and T. Heinzel 1997, *Metastability and spinodal points for a random walker on a triangle*, `cond-mat 9710287`, to appear in *J. Stat. Phys.*

[24] M. R. Evans, D. P. Foster, C. Godrèche and D. Mukamel 1995, *J. Stat. Phys.* **80** 69

[25] H. Z. Simon 1997, *Ph.D. thesis*, Bonn

[26] J. Krug 1991, *Phys. Rev. Lett.* **67** 1882

[27] B. Derrida, E. Domany and D. Mukamel 1992, *J. Stat. Phys.* **69** 667

[28] P. P. Martin 1991, *Potts models and related problems in statistical mechanics* (World Scientific, Singapore)

[29] M. R. Evans, D. P. Foster, C. Godrèche and D. Mukamel 1995, *Phys. Rev. Lett.* **74** 208

[30] R. B. Griffiths, C.-Y. Weng and J. S. Langer 1966, *Phys. Rev.* **149** 301; J. D. Gunton, M. San Miguel and P. S. Sahni 1989, in: *Phase Transitions and Critical Phenomena* Vol.8, p. 267, eds. C. Domb and J. L. Lebowitz (Academic Press)

[31] M. Le Bellac 1991, *Quantum and statistical field theory* (Oxford University Press, Oxford)

[32] M. den Nijs, in: *Proceedings of the 4th workshop on Statistical Physics, Seoul, January 1997*

[33] J. L. Lebowitz, E. Presutti and H. Spohn 1988, *J. Stat. Phys.* **51** 841

[34] K. Mallick 1996, *Ph.D. thesis*, Saclay

[35] C. H. Bennett and G. Grinstein 1985, *Phys. Rev. Lett.* **55** 657

[36] V. Privman and L. S. Schulman 1982, *J. Phys. A: Math. Gen.* **15** L238, and *J. Stat. Phys.* **29** 205

[37] C. Godrèche, J. M. Luck, M. R. Evans, D. Mukamel, S. Sandow and S. R. Speer 1995, *J. Phys. A: Math. Gen.* **28** 6039

[38] S. Sandow 1994, *Phys. Rev.* **E50** 2660

[39] U. Bilstein 1996, *diploma thesis*, Bonn

[40] R. Bulirsch and J. Stoer 1964, *Numer. Math.* **6** 413, M. Henkel and G. Schütz 1988 *J. Phys. A: Math. Gen.* **21** 2617

[41] M. N. Barber 1983, *Finite-size scaling*, in: *Phase Transitions and Critical Phenomena, Vol. 8*, eds. C. Domb and J. .L. Lebowitz (Academic,Press, N.Y.)

[42] N. G. van Kampen 1981, *Stochastic Processes in Physics and Chemistry* (North-Holland, Amsterdam)

[43] C. W. Gardiner 1990, *Handbook of Stochastic Methods for Physics, Chemistry and the Natural Sciences*

[44] P. F. Arndt, T. Heinzel and V. Rittenberg 1998, *J. Phys. A: Math. Gen.* **31** L45

[45] P. F. Arndt, C. Godrèche, T. Heinzel and V. Rittenberg 1998, *Spontaneous breaking of translational invariance and Bose-Einstein condensation in one-dimensional stationary states on a ring*, in preparation